JOURNAL OF QUATERNARY SCIENCE (2025) **40**(1) 153–173 ISSN 0267-8179. DOI: 10.1002/jqs.3661

JQS Journal of Quaternary Science QRA Quaternary Research Association

Palaeoenvironmental evolution and decline of the harbours of the Roman and Early Byzantine city of Elaiussa Sebaste (southeastern Turkey): natural and anthropic causes

ROMANA MELIS,[1]* EMANUELA BORGIA,[2] SAMUELE AGOSTINI,[3] ALESSANDRA CELANT,[4] FEDERICO DI RITA,[4] EMANUELE FORTE,[1] GIANGUIDO SALVI[1] and ESTER COLIZZA[1]

[1]Dipartimento di Matematica, Informatica e Geoscienze, Università di Trieste, Trieste, Italy
[2]Dipartimento di Scienze dell'Antichità, Sapienza Università di Roma, Roma, Italy
[3]Istituto di Geoscienze e Georisorse, Consiglio Nazionale delle Ricerche (IGG-CNR), Pisa, Italy
[4]Dipartimento di Biologia Ambientale, Sapienza Università di Roma, Roma, Italy

Received 9 May 2024; Revised 1 October 2024; Accepted 8 October 2024

ABSTRACT: The ancient city of Elaiussa Sebaste, currently Ayaş, is located on the southeastern coast of Turkey. It was one of the main trading Mediterranean harbours from the Augustan period until the early Byzantine era. The Arab invasion in the 7th century CE marked its definitive abandonment. A significant historical topic concerns the palaeoenvironmental evolution of the northern and southern harbours of Elaiussa Sebaste, including their decline and burial. An interdisciplinary study analysed six cores drilled in the current plains corresponding to the former harbour basins. A geoelectrical study, integrated with borehole stratigraphy, reconstructed the geometry of the carbonate bedrock that forms the accumulation base of the marine sediments. Sediments deposited from the 8th century BCE to the 6th century CE include the development phases of the ancient city from the 3rd century BCE onwards. Sedimentology, micropalaeontology (foraminifers, ostracods), palaeobotany (pollen, non-pollen palynomorphs, microcharcoals, plant macroremains) and Pb isotopes provided a model of the environmental evolution in both harbour basins. The main harbour expansion phase, marked by a change in Pb concentration, is hypothesized to have occurred between 140 and 220 CE, which is consistent with the historical sources indicating the development of the city during the mid-Roman Imperial period. © 2024 The Authors *Journal of Quaternary Science* Published by John Wiley & Sons Ltd.

KEYWORDS: harbour geoarchaeology; historical evolution; micropalaeontology; Roman and Byzantine age; sedimentology; Turkey

Introduction and historical context

The geoarchaeological study of Mediterranean ancient harbours has developed over the last two decades (see Morhange et al., 2015, 2016; Pint et al., 2015; Salomon et al., 2016; Stock et al., 2016; Giaime et al., 2019; Kaniewski et al., 2022). Ancient harbour basins are significant geoarchaeological and geochemical archives. Their sedimentary successions contain sedimentological and biogeochemical proxies that are useful in palaeogeographical reconstructions of past environmental changes (Marriner and Morhange, 2006a; Marriner et al., 2014; Morhange et al., 2015; Amato et al., 2020; Desruelles et al., 2023). Interdisciplinary geological disciplines such as sedimentology, palaeontology, palynology, geochemistry and geophysics are increasingly applied in archaeological research, providing tools to define the ancient environments influenced by natural and anthropic processes (e.g. Bernasconi et al., 2006; Marriner and Morhange, 2007; Algan et al., 2011; Mazzini et al., 2011; Stock et al., 2013, 2020; Seeliger et al., 2014; Melis et al., 2015; Morhange et al., 2015, 2016; Di Donato et al., 2017; Giaime et al., 2019; Amato et al., 2020, 2021; Ghilardi, 2021; Di Rita et al., 2022; Desruelles et al., 2023; Susini et al., 2023).

*Correspondence Romana Melis, as above.

E-mail: melis@units.it

At the end of the Holocene transgression, when sea level stabilized about 6000–7000 years ago (Lambeck and Purcell, 2005), Mediterranean civilizations began to settle along more stable coastlines (Benjamin et al., 2017 and references therein). During the Greek and Roman periods, several ancient settlements were located along the central–eastern Mediterranean coasts (Marriner and Morhange, 2007; Marriner et al., 2014; Giaime et al., 2019). Due to global sea level variations since the last glaciation, ancient harbours are now typically submerged or landlocked, often distant from the current coastline due to evolution of the coast. This results from recent tectonism, strong siltation, and extreme events such as floods and storms (Amato et al., 2021 and references therein).

Geological and archaeological aspects converge in Elaiussa Sebaste, an ancient port city on the southeastern coast of Anatolia, near modern Ayaş-Kumkuyu (about 60 km west of Mersin, Turkey). Research here aims to interpret the late Quaternary environmental and climatic evolution identifying natural and anthropic events. Elaiussa Sebaste was a crucial trade-port of ancient Cilicia, abundant in natural resources (in particular wood, olives and vines) and strategically located at a crossroads of Syria, Egypt, Cyprus and the Anatolian peninsula. It was founded during the Late Hellenistic period, in the 2nd–1st centuries BCE, on a naturally defended rocky promontory surrounded by two wide natural bays, later transformed into harbours. Elaiussa, granted the title of Sebaste in the age of Augustus, flourished greatly during the Early and Middle

Roman Imperial age, reaching its apogee during the Antonine (2nd century CE) and Severian (late 2nd–3rd centuries CE) ages. This development was halted with the invasion of the Persian king Shapur in 260 CE and repeated invasions by Isaurian tribes in the 4th and 5th centuries CE. Despite this, the ancient city maintained its prestige until the early 7th century CE. Arab invasions in the mid-7th century CE probably led to the city's decline and its abandonment.

Archaeological investigations at Elaiussa Sebaste have been conducted since 1995 by the Department of Antiquities of Sapienza University of Rome (Italy). Excavations over the last three decades (Equini Schneider 1999, 2003, 2007, 2010; Polosa et al., 2019; Barbanera, 2022) have provided extensive data, allowing for the diachronic reconstruction of the ancient city. These expeditions uncovered several monumental complexes from the Roman and Early Byzantine periods (Fig. 1).

The morphological characteristics of the coastal area undoubtedly contributed to the city's historical evolution. Two harbour environments were built due to the availability of two natural bays surrounding the rocky promontory to the north and south. The northern one was the most important because it was protected from the prevailing winds and occupied a deep bay protected by a pier in *opus caementicium*. It was also marked by a lighthouse, the possible remains of which were identified on the northern tip of the promontory (Fig. 1). The southern port basin is less well known from an archaeological point of view. During historical times, the two harbours were separated by an isthmus that probably did not emerge during prehistoric times (Toro and Di Filippo, 1999). The formation of the isthmus was significant for the historical evolution of the area, as it connected the promontory's quarters with the mainland.

During the Imperial period, the Northern Harbour (hereafter NH) had a monumental front and served a representative function, being the most important and well-protected basin. In contrast, the Southern Harbour (hereafter SH) served mainly commercial purposes (Tempesta et al., 2020). The coastal environment around the city has been continuously affected by both human activities and, probably, natural events. Today the ancient ports of Elaiussa Sebaste are landlocked and completely buried due to extensive coastal development after their abandonment.

The first geoarchaeological investigation of Elaiussa Sebaste focused on studying a core located in the NH (core ELA6, Melis et al., 2015) where preliminary results suggested a hypothetical scenario linking the harbour evolution to natural and human influences. To enhance understanding of this initial palaeoenvironmental reconstruction, we present a study of six additional cores located in the two harbours (Fig. 1), integrated by geophysical studies to frame the results in a broader scenario. The aim of this research is to provide new data by combining historical, archaeological and multidisciplinary geological disciplines for a comprehensive interpretation of the environmental evolution recorded in the harbour basins, inserting this within the historical context of use. The integration of these data is mainly directed at verifying hypotheses about the disappearance of Elaiussa's ancient harbours, whether natural or anthropogenic.

Study area: geological and geomorphological setting

The southern coast of Turkey is located in the eastern extension of the Aegean arc, on the southern piedmont of the Taurus Mountains chain. Roughly N–S extending faults were active during the Quaternary, indicating the complex nature of tectonics along the coastline (Desruelles et al., 2009 and references therein).

Desruelles et al. (2009) studied the southeast coast of Turkey in order to define sea level changes since the Middle Holocene. Using beach rocks, they evidenced variable tectonic subsidence in south and southeast Turkey over the last 2800 years, with phases of instability and subsidence in the Finike area, where archaeological Roman remains are today located at −1.5 m (Fouache et al., 2005; Desruelles et al., 2009), and relative sea level stability toward the Iskenderun Gulf. More specifically, from Alanya to Viransehir, the area was uplifted by about +0.5 m probably before the 12th century CE (Fouache et al., 2005; Desruelles et al., 2009). Tectonic uplift phases, probably of seismic origin, caused several raised shorelines around 2500 and 1400 a BP along the Hatay coast, between Turkey and Syria (Pirazzoli et al., 1991). In the Elaiussa Sebaste area, evidence of Late Holocene tectonic uplift of about 1.2 mm a^{-1} for the last 1000 years was found by dating different sea level markers (fossil shells of *Patella* cf. *aspera*) collected 1 m above their natural living environment (Cosentino et al., 2016).

This settlement developed along a coastal belt with modest hills, plains and a promontory for a total area of 23 ha within the Mersin region (Fig. 1). Two harbours dating to the Roman–Byzantine periods were built on a coastal area consisting of well-stratified Middle Miocene limestones of the Mut Formation, which outcrop extensively in the coastal area from Silifke to Erdemli as a part of the Mut Basin (Şafak et al., 2005; Cosentino et al., 2012: see fig. 1c, Elaiussa Sebaste is located to the east of the 34th parallel). These beds slope gently (5°–10°) southwards and constitute the harbours' bedrock. The eastern side of the ancient NH presents rocky shorelines with sub-vertical walls. Previous geological studies of the Elaiussa Sebaste area by Toro and Di Filippo (1999), Ballirano et al. (2003), Di Filippo and Toro (2003) and Melis et al. (2015) revealed the complex relationships between tectonics, erosion and sedimentation.

Today, two plains with elevations not exceeding 2 m above sea level occupy the area of the ancient harbours, which have completely silted up. The most recent deposits consist of sands–silts mainly of aeolian origin, coming from the north, together with '*colluvium*' sediments which are overlaid by '*terra rossa*' (Toro and Di Filippo, 1999; Di Filippo and Toro, 2003). A sandy dune presently covers a relatively large sector of the calcareous promontory.

Materials and methods

In 2012, six continuous drill cores (ELA2, 3, 4, 5, 7, 9) from 5.0 to 14.1 m in length were recovered from both the northern (ELA2–ELA7) and southern (ELA9) ancient harbours (Fig. 1, Table 1). Drilling was performed with a modular and portable rotary drilling machine for micro-piles and coring with a core diameter of 0.07 m. All cores were GPS-levelled and their depths referenced to modern mean sea level (msl). The core site surface elevations range from 0.98 to 1.87 m above msl (Table 1). In 2013, within the framework of the same project, a geophysical survey combined ground-penetrating radar (GPR), giving a total of 430 m of profiles and electrical resistivity tomography (ERT), giving a total of 850 m of profiles.

The cores were split in half, described and sampled at the Department of Mathematics, Informatics and Geosciences of the University of Trieste. Sediment cores were sub-sampled at a mean resolution of 50–80 cm, depending on the nature of the facies. Sixty bulk samples (~50 cm^3, corresponding to 2-cm-thick core sections) were examined for grain size, organic carbon and total nitrogen content, and microfossils.

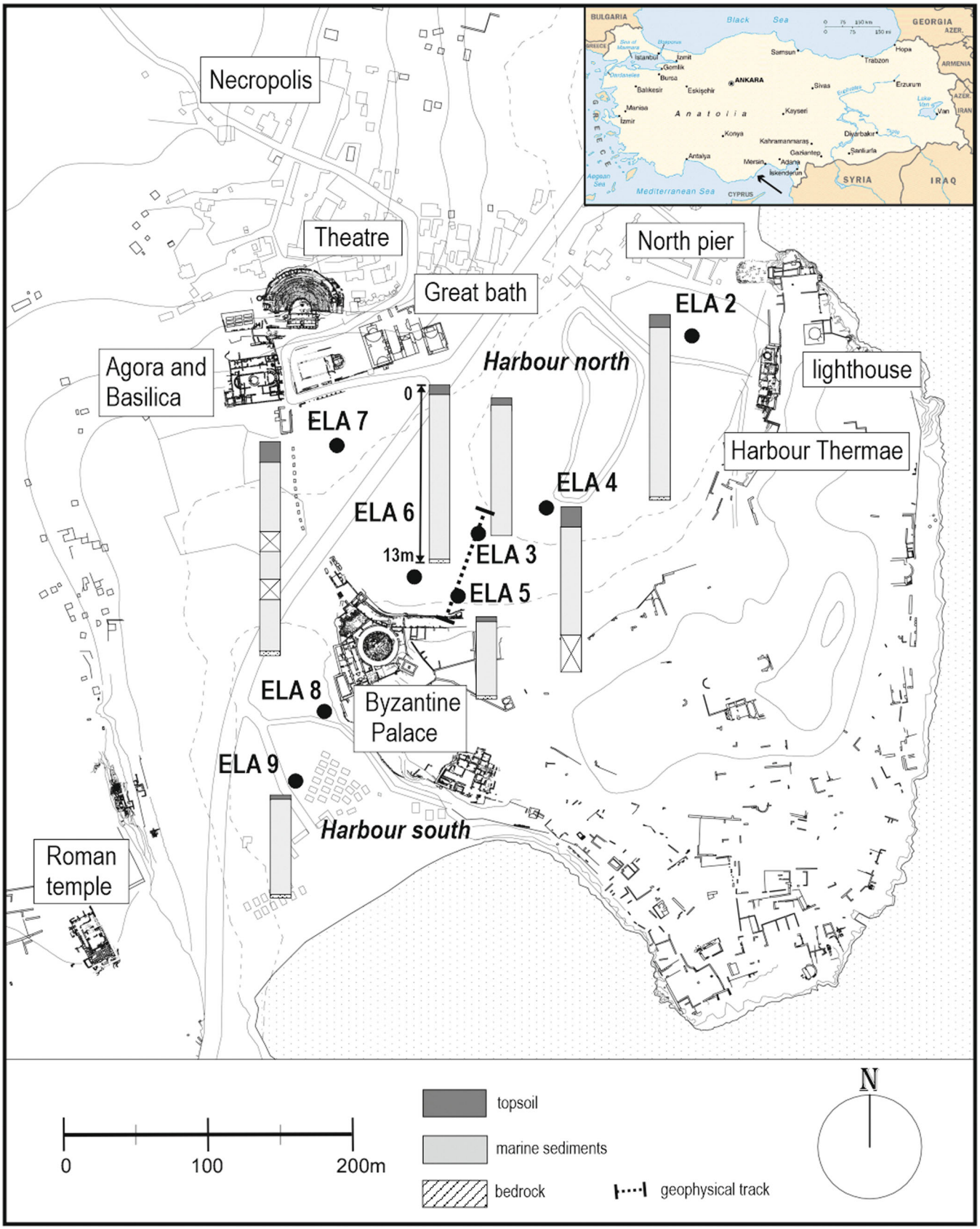

Figure 1. Geographical location of Elaiussa Sebaste including the main historical monumental complexes, the location of the cores and the two harbours discussed in the text. [Color figure can be viewed at wileyonlinelibrary.com]

The chronology of the cores is based on 13 accelerator mass spectrometry (AMS) radiocarbon dates from plant macroremains (charcoal fragments) analysed at the CIRCE (Centre for Isotopic Research for Cultural and Environmental heritage) laboratory at Caserta (Italy). One level (ELA7.10) was dated using benthic foraminifera at the Poznań Radiocarbon Laboratory (Poland). The software Bacon v.2.5.5 was used to elaborate the age–depth models for cores ELA5, ELA6

Table 1. List of studied cores, geographical coordinates, core length from the current surface and core depth below current mean sea level (m bsl).

Core	Latitude N	Longitude E	Length (m)	Depth bsl (m)
ELA2	36°29.013	34°10.610	13.5	12.3
ELA3	36°28.933	34°10.510	10.0	8.6
ELA4	36°28.941	34°10.540	10.5	8.6
ELA5	36°28.914	34.10.505	6.0	4.6
ELA6*	36°28.914	34°10.482	13.0	11.73
ELA7	36°28.970	34°10.448	15.5	14.3
ELA9	36°28.848	34°10.432	6.0	5.0

*The core studied by Melis et al. (2015).

and ELA7 through a Bayesian approach (see Supporting Information Fig. S1).

The grain size of each sample was determined using a Malvern Mastersizer Hydro2000S Diffraction Laser unit for the <2-mm size fraction. The gravel content was determined using an optical microscope. Sand and mud classes were determined using the Udden–Wentworth (Wentworth, 1922) grain-size classification. Grain-size parameters were determined using the formulas of Folk and Ward (1957). Total organic carbon (C_{org}) and total nitrogen (N_{tot}) content were determined as the mean value of two replicates of the same samples using an ECS 4010 CHNSO elemental analyser and acetanilide as the calibration standard. Before analysis, the samples were gradually acidified with 0.1–1.0 M HCl (Hedges and Stern, 1984).

Foraminifera were examined in the sandy fraction (>63 μm) of 60 samples from cores ELA2, 3, 4, 5, 7 and 9, while ostracods were examined in the sandy fraction of 39 samples from cores ELA2, 5 and 7.

The foraminiferal and ostracod data were reported as relative abundance (%). Faunal density (FD) was calculated as the number of specimens per gram of total dry sediment (specimens g^{-1}). Shannon diversity index (H) was calculated for ostracods. Foraminifer and ostracod data from Melis et al. (2015) were taxonomically aligned and included in the dataset for global interpretation. Their relative frequency was analysed with an orthogonal rotated (Varimax) Q-mode principal component analysis (PCA) using the XLSTAT software, v.2020-3.1.

Pollen analysis of core ELA6 reported in a previous study (Melis et al., 2015) was upgraded by including new non-pollen palynomorph (NPP) and microcharcoal data. In addition, pollen, NPP and microcharcoal analyses were carried out on three samples of core ELA5. Chemical treatment for pollen extraction followed standard procedures according to Faegri and Iversen (1989). Microcharcoal analysis of cores ELA5 and ELA6, aimed at reconstructing the fire history of the site, followed the procedures described by Clark (1982). Charcoal macro-remains were identified using a Zeiss Axiolab 5 metallographic microscope (×50–500) and atlases of wood anatomy (Schweingruber, 1990; Akkemik and Yaman, 2012).

A geochemical investigation to detect concentrations of Al and Pb was carried out on nine levels of the previously published ELA6 core. This core has been considered the reference sequence for these settings due to its completeness and location (Melis et al., 2015). After total decomposition, the treated sediments were analysed by inductively coupled plasma-atomic emission spectroscopy (ICP-AES) using a Spectroflame Modula E instrument by SPECTRO® of the Department of Chemical and Pharmaceutical Sciences of the University of Trieste. The crustal enrichment factor (EF) was calculated as the Pb/Al ratio, Al being a major crustal component (McLennan, 1995). The same samples from core ELA6 were selected for determination of the Pb radiogenic isotopes by thermal ionization mass spectrometry at the Istituto di Geoscienze e Georisorse of CNR (Italian National Research Council) of Pisa (Italy) using a Finnigan MAT 262 multi-collector mass spectrometer running in static mode.

For more detailed methodology, see the Supporting Information.

Results

All the cores were of satisfactory quality, with continuous recovery in most cases (ELA2, 3, 5 and 9; Fig. 1). For two stations (ELA5 and ELA7), large clasts and the underground aquifer created a recovery gap. The lithostratigraphy of the cores is reported in Fig. 2; of 74.5 m of pipes used for the borings, sediment recovery exceeded 90%. Miocene limestone bedrock was reached in cores ELA5 (6.0 m), ELA6 (13.0 m), ELA7 (15.2 m) and ELA9 (7.5 m) (Fig. 2). All depths mentioned in the text are expressed in metres below mean sea level altitude (hereafter m bsl).

Most sediments have a predominant sandy component which takes on a yellowish/oxidized colour at superficial levels. In all the surveys, however, mud levels darker in colour and sometimes rich in plant remains and charcoal were found. Remains of ceramic material (generally shards of amphorae) indicating human presence were found during sampling (Fig. 2). The calibrated radiocarbon ages indicate that the sediments overlying the calcareous bedrock date from the 8th century BCE to the 5th century CE (Table 2).

Geophysical survey

The overall quality of ERT data is quite high, with standard deviations above 5% for repeated measurements taken with the same electrodes only for 1.2% of the whole dataset, and limited to the Dipole–Dipole configuration which showed an overall lower signal to noise ratio. The inverted profiles show high and coherent resistivity contrasts between different geo-hydrological units (Fig. 3). Below a high-resistivity layer, 1.5–2 m thick and interpreted as unsaturated soil and sediments, there is an abrupt and laterally continuous resistivity change interpreted as the water table (WT) (Fig. 3). At variable depths, decreasing towards the south, the relatively higher resistivity marks the zone of the limestone bedrock (L). This perfectly matches the borehole stratigraphy. The above-described trend is quite similar in both the NH and SH; a slightly different situation was found only in the northern portion of the study area (Fig. 3b′). In fact, while the vertical resistivity trend is similar to the other areas (see Fig. 3a, b′, b″) the resistivity range is smaller and shifted towards lower values (1–100 Ωm). Below the interpreted WT, sediment resistivity is mostly less than 40 Ωm and often less than 10 Ωm, testifying to brackish water near the actual topographic surface. The bedrock has an irregular surface, reaching over 16 m deep about 30 m west of borehole ELA2 and just 4 m below the topographic surface in the central part of the westernmost profile.

Combining: (i) all bedrock depths extracted from inverted ERT profiles by an automated procedure which picks the local higher resistivity gradient, (ii) the depth information of the boreholes reaching the bedrock (i.e. ELA5, 6, 7 and 9) and (iii) the limits of the outcropping limestone (i.e. by definition the zones with limestone at zero depth), we obtained a map showing the depth of the bedrock in both

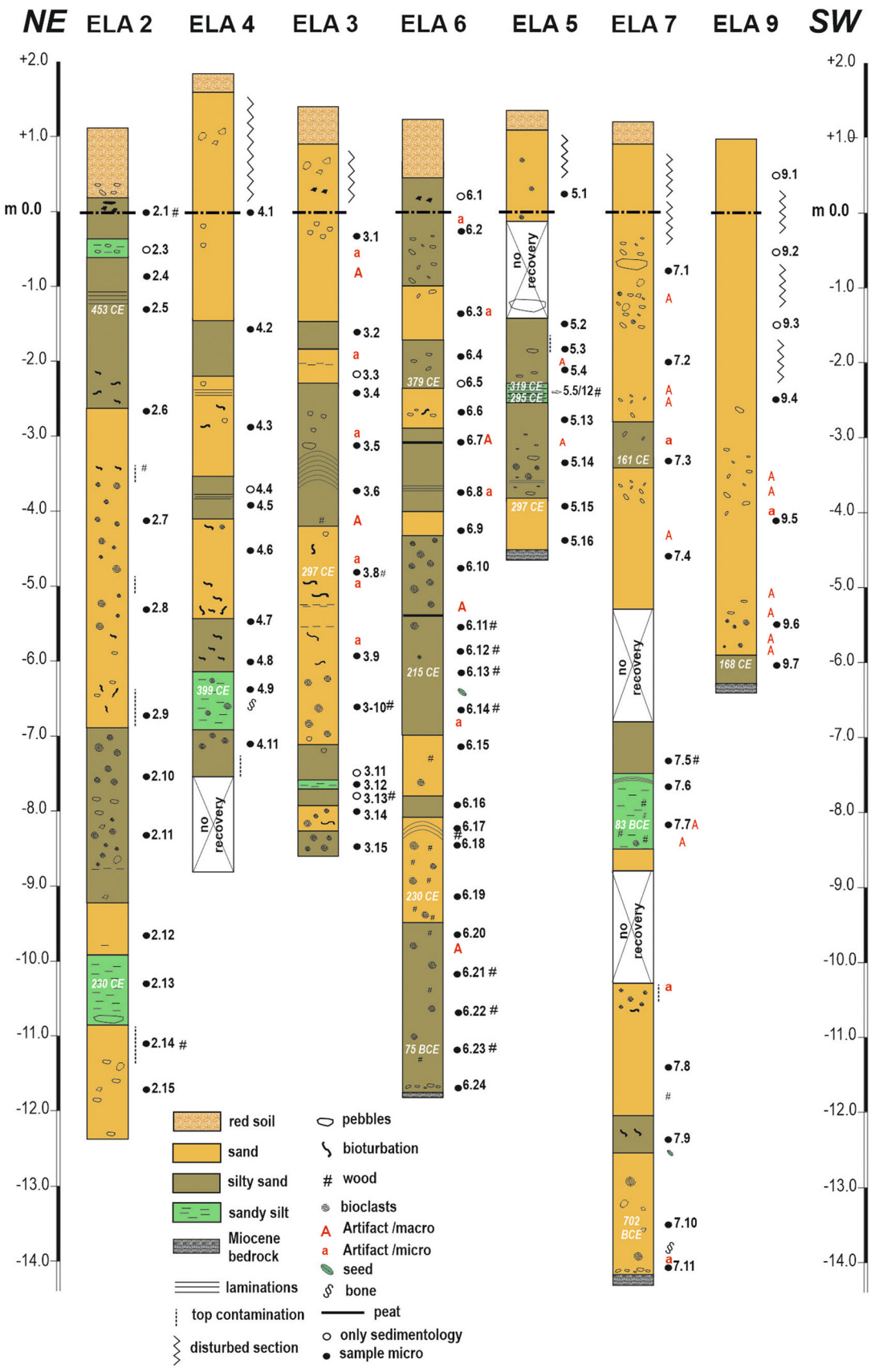

Figure 2. Lithostratigraphy of the studied cores, represented by locations from NW to SE. Studied samples (black dots) and calibrated dating (white inside the cores) are reported. The depth of the cores is calculated in relation to the current mean sea level and reported in the text as metres below sea level (m bsl). [Color figure can be viewed at wileyonlinelibrary.com]

the NH and SH (Fig. 4). The map shows an uneven data distribution, particularly a lack of data in the western portion of the SH. However, some interesting information is still obtainable.

The NH has a greater depth to bedrock than the SH, exceeding 16 m in its southern part. Below the actual isthmus, a shallow bedrock threshold separates the two harbours. Although limited data in the SH restrict detailed

Table 2. AMS radiocarbon data from the studied cores. The calibrated calendar ages ±2σ are reported in years BP and BCE/CE. The calendar ages are calibrated using the Calib v.8.2 software with the IntCal20 and Marine20 calibration (evidenced by the asterisk) curves. See Supporting Information for details. Calibrated age ranges are at 95% confidence.

Sample ID	Lab. code	Core level	Depth (m bsl)	Material	^{14}C age (a BP)	δ^{13}C	Calibrated age (cal a BCE/CE)	Median prob. (cal a BCE/CE)
TS_2	DSH5321	ELA2.5	1.2	Charcoal	1633 ± 25	−13	402–538 CE	453 CE
TS_1	DSH5320	ELA2.13	10.2	Charcoal	1820 ± 30	−28	152–256 CE	230 CE
TS_3	DSH5322	ELA3.8	4.8	Charcoal	1771 ± 35	−36	215–380 CE	297 CE
TS_5	DSH5324	ELA4.9	6.4	Charcoal	1663 ± 43	−24	327–482 CE	399 CE
TS_6	DSH5325	ELA5.6	2.4	Charcoal	1742 ± 34	−33	244–383 CE	319 CE
TS_7	DSH5326	ELA5.12	2.5	Charcoal	1770 ± 56	−24	200–414 CE	295 CE
TS_4	DSH5323	ELA5.15	4.0	Charcoal	1771 ± 36	−29	214–381 CE	297 CE
TS_8	DSH5327	ELA6	2.2	Charcoal	1679 ± 34	−33	324–435 CE	379 CE
TS_10	DSH5329	ELA6.13	6.2	Charcoal	1834 ± 27	−27	126–251 CE	215 CE
TS_11	DSH5330	ELA6.19	9.1	Charcoal	1820 ± 27	−32	154–256 CE	230 CE
TS_12	DSH5331	ELA6.23	11.2	Charcoal	2064 ± 33	−23	168 BCE to 18 CE	75 BCE
TS_9	DSH5328	ELA7.3	3.3	Charcoal	1877 ± 53	−29	24–252 CE	161 CE
TS_13	DSH5332	ELA7.7	8.2	Charcoal	2071 ± 33	−27	172 BCE to 12 CE	83 BCE
ELA7	Poz-158887	ELA7.10	13.5	Foraminifers	3075 ± 35		918–441 BCE*	702 BCE
TS_15	DSH5334	ELA9.7	6.1	Charcoal	1876 ± 30	−35	113–237 CE	138 CE

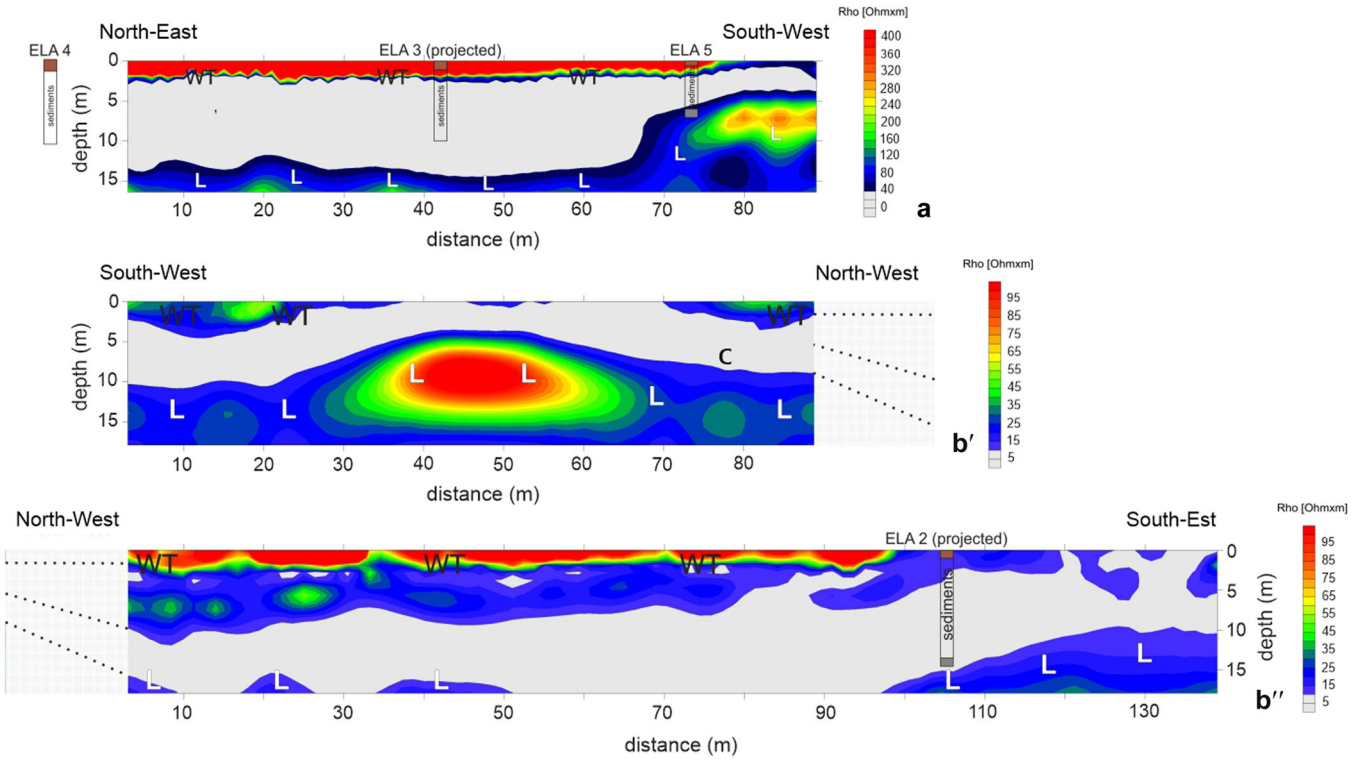

Figure 3. ERT interpreted profile 1 (a) and 2 and 3 (b′ and b″) with superimposed schematic stratigraphy of boreholes ELA 3 (projected), ELA 4, ELA 5 and ELA 2 (projected). Brown and grey colours in the stratigraphy represent the topsoil and limestone, respectively. WT: water table; L: limestone. Location given in Fig. 4. [Color figure can be viewed at wileyonlinelibrary.com]

morphological analysis, it is noteworthy that the bedrock's maximum depth of 10.5 m is unexpectedly close to the isthmus and the outcropping limestone onshore.

Sediment texture

The sediments range from sand to silty sand and sandy silt; the sand content varies from 31.4 to 97.2% (average 72.0 ± 15.4%) and the silt from 2.8 to 58.7% (average 21.8 ± 12.8%), while the clay content ranges from 0.0 to 17.0% (average 6.2 ± 3.7%) (Table S1). The sediments are generally poorly and very poorly sorted; sorting (Sort) increases in the sandy sediments (Table S1). In the sand fraction, fine to very fine sands prevail (Fig. 5). All cores show a coarsening-up trend in the recent sediments with an increase in fine sand (ELA5 and ELA7), medium and fine sand (ELA2, 3 and 4), and medium and coarse sand (ELA6 and ELA9) (Fig. 5). In almost all the cores the gravel fraction comprises a suite of different materials, such as marine molluscs, wood fragments, charcoals, lithogenic grains and ceramic shards. These ceramic shards are more abundant in cores ELA6 and ELA7 located in the NH. The sediments are

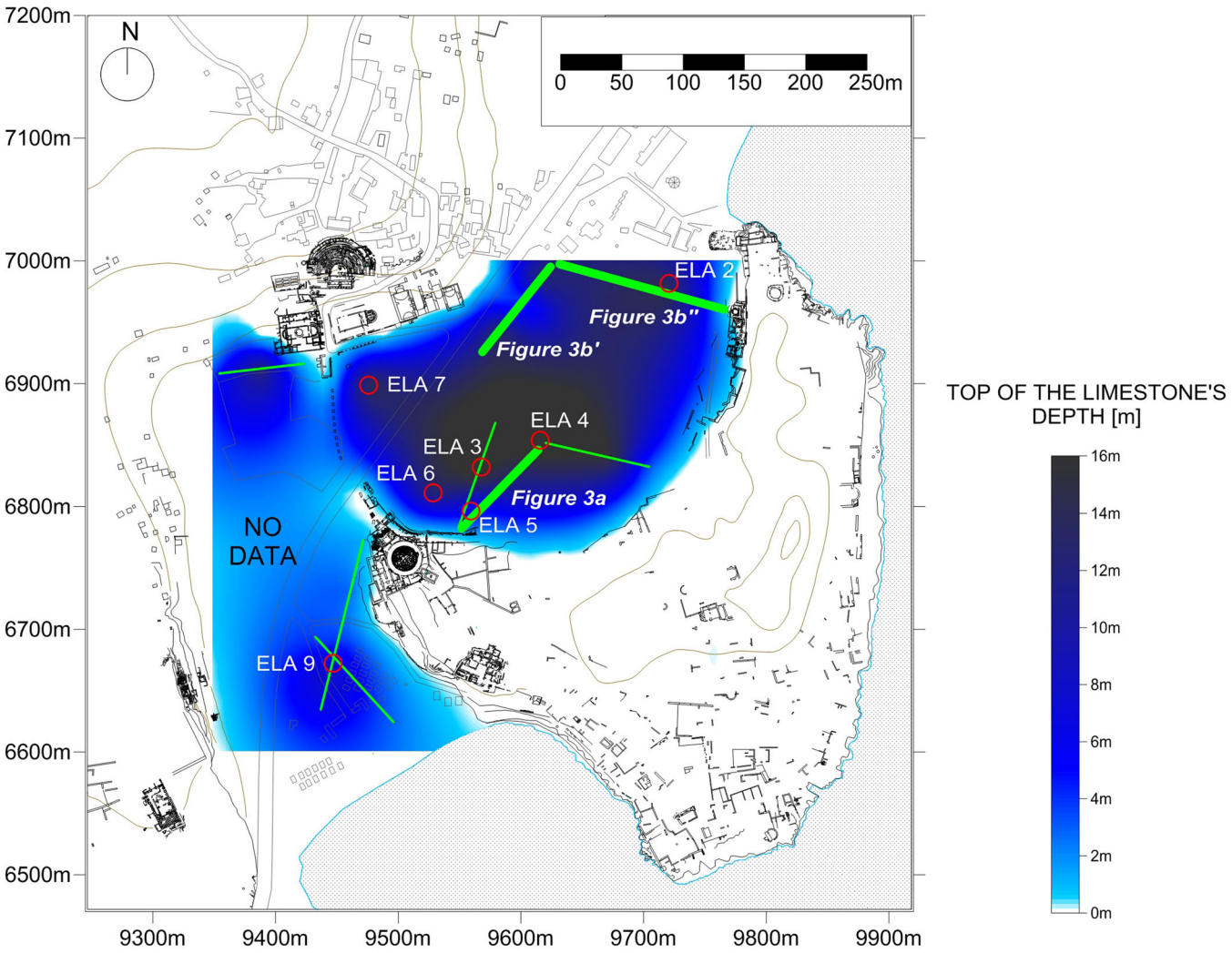

Figure 4. Map of the depth of the bedrock from integrated ERT, borehole and limestone outcrop data. Green lines show the location of ERT profiles; thicker green lines mark profiles shown in Fig. 3a (profile 1) and Fig. 3b′ and b″ (profiles 2 and 3). [Color figure can be viewed at wileyonlinelibrary.com]

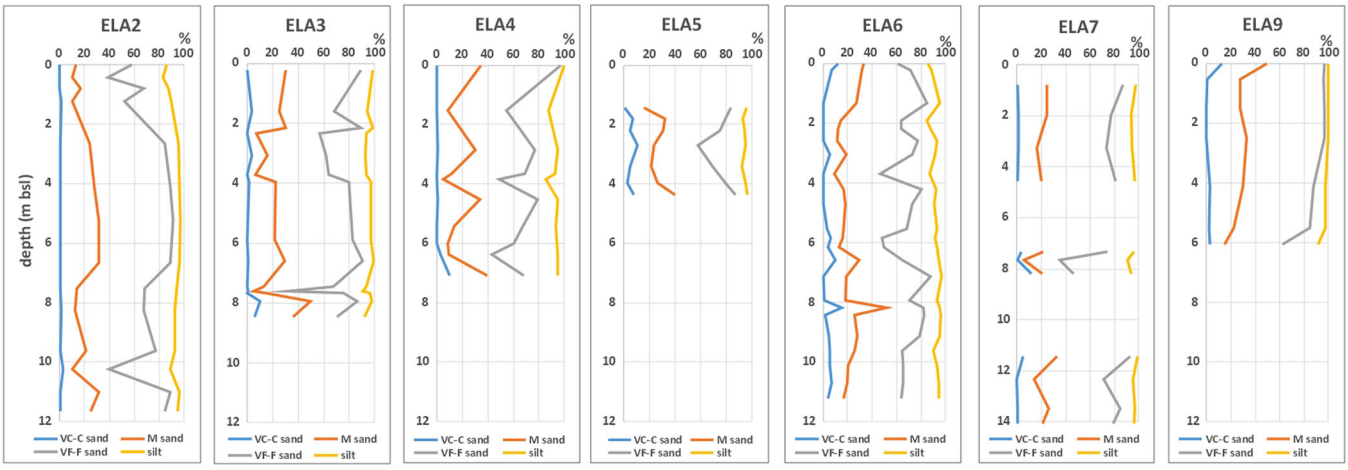

Figure 5. Sediment texture of the studied cores with depth. The percentages of VC-C (very coarse–coarse), M (medium) and VF-F (very fine–fine) sand and silt are cumulatively reported. [Color figure can be viewed at wileyonlinelibrary.com]

mostly structureless, though some limited portions are laminated. Some bioturbation is also seen.

Organic matter

Organic carbon content (C_{org}) is generally below 1.0%, but each core shows one or, in some cases, more levels with values exceeding 2.0%, with a maximum of 10.3% in core ELA5 (Table S1). These higher values are associated with increased charcoal and wood fragments, as already evidenced in core ELA6 (Melis et al., 2015). Total nitrogen (N_{tot}) usually measures less than 0.14% and, as a rule, correlates with C_{org}, except in core ELA3. The molar ratio $C_{org}/N_{tot} < 10$ suggests marine organic matter for most studied levels, except for core

ELA5, where all C_{org}/N_{tot} values are >10 (Table S1). C_{org}/N_{tot} values > 10 usually correspond to the increased values of C_{org} in the sediments, suggesting a continental origin of the organic matter (e.g. Goñi et al., 2003). This is particularly evident in cores ELA6, ELA7 and mainly ELA5, located in the NH near the ancient coastline.

Foraminifera

Foraminifera species identification follows the Mediterranean systematic studies of Cimerman and Langer (1991), Sgarrella and Moncharmont Zei (1993), Meric et al. (2004, 2008, 2014), and Milker and Schmiedl, (2012). Hayward et al. (2021) was used to recognize *Ammonia* species. Specific names adhere to the World Register of Marine Species (WoRMS, 2024). The interpretation of Holocene foraminifera assemblages is based on comparisons with ecological data from various modern Mediterranean coastal regions (e.g. Jorissen, 1987; Albani et al., 1991; Sgarrella and Moncharmont Zei, 1993; Donnici and Serandrei Barbero, 2002; Amorosi et al., 2004; Meriç et al., 2004; Melis and Covelli, 2013).

The 82 examined samples contain 88 foraminifera species pertaining to 43 genera, with *Bolivina* reported as spp. (Table S2). The assemblage is generally rich and diverse, primarily featuring porcelaneous (around 60% frequency) and hyaline taxa, with occasional agglutinated taxa. The most frequent foraminifers are species of *Ammonia* and *Elphidium*, hyaline taxa, and *Adelosina*, *Cycloforina*, *Quinqueloculina*, *Sinuloculina* and *Triloculina* among the porcelaneous taxa (Table S2). Selected species were imaged using a Zeiss Gemini 300 FEG scanning electron microscope at the University of Trieste (Plates S1 and S2). Four principal component (PC) scores explain 89.3% of the total variance in the data set. These PCs, termed foraminiferal assemblages (FAs) after the dominant taxa, represent distinct ecological conditions, interpretation of which is reported in Table 3.

Ostracods

All ostracod specimens were identified using Mediterranean benthic ostracod systematic literature (Bonaduce et al., 1976, 1980; Breman, 1976; Yassini, 1979; Aiello and Barra, 2010) and, in particular, papers relating to the eastern Mediterranean (Athersuch, 1979; Kılıç et al., 2000; Kiliç, 2001; Kubanç, 2003; Colin et al., 2005; Meric et al., 2008; Perçin Paçal, 2011; Tsourou, 2012). Of 62 samples, 54 contained ostracod fauna, consisting of 60 species, 10 of which recorded in open nomenclature. Some species had few specimens, while others were more numerous. Faunas are usually well preserved. The most abundant species pertain to the genera *Aurila*, *Loxoconcha*, *Urocythereis* and *Xestoleberis* (Table S3).

Four PC scores in this study explain 73.3% of the total variance in the ostracod data. Each PC is defined by species with the highest positive PC scores. In three cases, they are accompanied by taxa with lower but significant scores (Table 3). These species were identified using a Zeiss Gemini 300 FEG scanning electron microscope at the University of Trieste (Plate S3). In the following discussion, the calculated PCs referred to as ostracod assemblages (OAs) using the name of the dominant taxa represent distinct ecological conditions, interpretation of which is reported in Table 3.

Pollen and wood analysis

Core ELA6 displays arboreal pollen (AP) percentages from 45% to 59% mainly related to *Pinus* and evergreen woody taxa, such as *Olea*, *Phillyrea*, *Quercus* evergreen and Ericaceae. Among herbaceous taxa, Poaceae, Brassicaceae, Cichorioideae, Chenopodiaceae, Cyperaceae/Juncaceae, *Sarcopoterium* type and Asteroideae stand out. Anthropogenic indicators include a few woody and herbaceous taxa, mainly *Vitis*, *Juglans* and cereal type. The NPP record includes significant amounts of foraminiferal linings, *Glomus*, *Sporormiella* and *Trichuris* (Figs. 6 and 7).

The pollen record of core ELA5 shows slightly higher AP percentages (55–67%) than ELA6 (Figs. 6 and 7). *Pinus*, accompanied by *Olea*, Ericaceae and *Quercus* evergreen, are still the main pollen contributors among trees and shrubs. Herb taxa are mostly composed of Cyperaceae/Juncaceae, Poaceae, Cichorioideae, Chenopodiaceae, Asteroideae and *Sarcopoterium* type. Anthropogenic indicators include high values of cereal type and a moderate presence of *Juglans*. The most significant NPPs are fungal spores of *Sporormiella*, *Sordaria* and *Glomus*, as well as eggs of the intestinal parasites *Trichuris* and *Ascaris* (Figs. 6 and 7). Charcoal fragments, retrieved from ELA5, ELA6 and ELA7, are poorly preserved and mostly do not exceed 2 mm. However, it was possible to identify charred fragments of pine, which might be ascribed to *Pinus brutia*, according to the anatomical features reported by Akkemik and Yaman (2012).

Geochemistry and Pb isotope composition

In core ELA6, Pb and Al contents range from 5.6 to 74.4 ppm (average 26.3 ± 23.6. ppm) and from 4.4 to 10.0% (average $7.4 \pm 1.8\%$), respectively. The Pb content peaks around 8 m bsl, and then decreases toward the top of the core, except for a rise at 3 m bsl (Table S4). The EF (Pb/Al) distribution mirrors the Pb concentration pattern, showing a significant increase at about 6.6–8 m bsl (Table S4). The three Pb isotopic ratios also show a similar trend: $^{208}Pb/^{204}Pb$ ranges between 38.715 and 38.929 (average 38.789 ± 0.069), $^{207}Pb/^{204}Pb$ between 15.654 and 15.728 (average 15.675 ± 0.025), and $^{206}Pb/^{204}Pb$ between 18.632 and 18.756 (average 18.681 ± 0.047) (Table S4). Despite some data scattering, the isotopic Pb ratios show a marked decrease at 6.6–8 m bsl (Table S4).

Discussion

The multiproxy geoarchaeological study of the Elaiussa Sebaste area confirms that the sediments in both sectors historically identified as harbours (NH and SH) are from shallow-water marine palaeoenvironments.

Integrated geoelectrical surveys, stratigraphic analysis of the boreholes and limestone outcrops reveal the carbonate bedrock's geometry beneath the marine sediments. In the NH, two depocentres were identified, one near the port entrance and another further inland, both over 15 m deep and separated by a bedrock rise in the area in front of the monumental part of the city (Fig. 4). This rise may have constrained sediment mobility and influenced coastal currents during the period of activity of the NH. Similarly, the SH has two depocentres reaching 10 m deep, but their connection could not be confirmed due to highway obstruction preventing dedicated measurements (Fig. 1). The limestone close to the surface below the isthmus confirms that the two ports were definitely divided by this morphological feature (Fig. 4). The isthmus represented the connection between the first nucleus of the city on the promontory and its expansion on the mainland which occurred during the Early Imperial period (Equini Schneider, 1999).

The oldest radiocarbon age detected in the basal part (13.5 m bsl) of core ELA7 (NH) is 3075 ± 33 a BP (918–441 cal

Table 3. Ecological characteristics of the most significant species pertaining to the foraminiferal and ostracod assemblages (FAs and OAs) revealed by PCA and their interpretation. The percentage variance is reported for each PCA.

PCA assemblage	Variance (%)	Co-occuring taxa	Autoecology	Interpretation
Urocythereis spp. OA	32.2	*Aurila convexa*	The assemblage is characterized by a phytophilous genus widely distributed in the littoral and sublittoral zones of most Turkish coastlines and lagoonal waters, considered tolerant of a wide range of salinity (Mazzini et al., 2022 and references therein; D'Orefice et al., 2020 and references therein; Pint et al., 2015; Rossi et al., 2021)	This OA is represented, in particular, by the species *Urocythereis* cf. *britannica* together with *Aurila convexa*. This assemblage characterizes a phytal coastal environment indicating an upper vegetated infralittoral environment with variable salinity values (**Open Bay**).
Xestoleberis spp. OA	10.2	*Cistacythereis caelatura* and *Aurila* spp.	The species are common in Turkish coastal marine waters and are able to survive despite environmental and ecological changes. The high values mainly of *X. communis* and *X. dispar* indicate polyhaline conditions with substantial seawater inputs. Both species tolerate low oxygen levels (Vittori et al., 2015). They have also been reported as a dominant species in modern polluted water (Mazzini et al., 2011 and references therein; Salvi et al., 2015, 2020; Rossi et al., 2021)	This OA is dominated by the genus *Xestoleberis* (mainly *X. communis*) in association with *C. caelatura* and *Aurila* spp., and is used to represent shallow water environments with high variability of salinity values (**Open Bay**).
Cushmanidea turbida OA	20.5		Associated with transitional environments between marine and fresh waters and is characterized by a high tolerance to salinity variations and trophic gradients (Mazzini et al., 2011 and references therein; Aiello et al., 2020; Rossi et al., 2021; Mazzini et al., 2022 and references therein)	*Cushmanidea turbida* characterizes this OA. In this study it could record a back-barrier basin environment with variable salinity conditions and changeable rates of seawater exchange, such as typical of marine upper infralittoral waters, in moderately stressed environments or a sheltered bay (**Sheltered Bay**).
Loxoconcha spp. OA	10.3	*Leptocythere* spp. (mainly *Leptocythere levis*)	The two associated genera are often reported in vegetated lagoon and marine environments and are capable of tolerating muddy substrates, high organic matter inputs and slight oxygen deficiency (Carbonel, 1982; Barbieri et al., 2019 and references therein; Mazzini et al., 2022 and references therein)	This OA is dominated by the genus *Loxoconcha* (particularly *Loxoconcha rubritincta* and *L. stellifera*) together with *Leptocythere* spp. (mainly *Leptocythere levis*). In the studied cores, this OA is used to represent **s**heltered bay environments, connected to the sea and characterized by high inputs of organic material (**Sheltered Bay**).
Ammonia abramovichae FA	40.8		*Ammonia abramovichae* is a recently described species. Following Hayward et al. (2021), it belongs to the morphogroup *A. parkinsoniana* which is one of the dominant species in sandy sediments at inner shelf depths along the eastern Mediterranean coast (Elshanawany et al., 2011). Elsewhere along the same coast in Egypt, this species also lives in large enclosed, saline lagoons at shallow depths of less than 2 m (El Baz, 2017).	This FA is characterized by underrepresentation of the other taxa with negative PC scores. It generally coincides with sandy sediments. This is used to represent shallow water, unvegetated, high-hydrodynamic environments (**Open Bay**).
Elphidium pulvereum FA	9.5	*Haynesina germanica*, *Pseudotriloculina rotunda*, *Quinqueloculina seminulum*	The dominant species of this FA are considered as stress tolerant and euryhaline living in marginal, paralic, infralittoral and circalittoral environments (i.e. Sgarrella and Moncharmont Zei, 1993; Melis and Covelli, 2013; Langlet et al., 2014)	It is significant only in mud levels rich in organic C (charcoals). This FA is used to represent sheltered shallow water environments rich in organic matter (**Protected Bay**).
Peneroplis pertusus and *P. planatus* FA	35.5	*Adelosina* spp., *Quinqueloculina seminulum*	These porcelaneous taxa typically live in infralittoral vegetated settings (Sgarrella and Moncharmont Zei, 1993)	It is significant in several levels of all cores except ELA3 and behaves oppositely to the *A. abramovichae* FA. This FA is used to indicate well-lit environments populated by algae and marine phanerogams (**Open Vegetated Bay**).

(*Continued*)

Table 3. (*Continued*)

PCA assemblage	Variance (%)	Co-occuring taxa	Autoecology	Interpretation
Ammonia gr. *tepida* FA	3.5	*Adelosina carinatastriata*	*Ammonia* gr. *tepida* commonly occurs in sheltered, unvegetated, mid-low tidal and shallow (<3 m) subtidal, usually slightly hyposaline (~20–35 psu), muddy environments, globally (e.g. Murray, 2006; Hayward et al., 2021). It shows the highest concentrations in highly confined settings such as lagoons, estuaries, tidal flats, etc. (Jorissen, 1987; Albani et al., 1991; Sgarrella & Moncharmont Zei, 1993; Debenay et al., 2000; Melis & Violanti, 2006; Melis & Covelli, 2013).	It is significant in a few levels of cores ELA3, 4, 6 and 7 (Fig. S2) and is related to muddy sediments. This FA is used to represent sheltered shallow water environments with low and/or variable salinity (**Low Salinity Influence**).

BCE) (Table 2). No older sediments were found as the core reaches the bedrock at 14.2 m bsl (Fig. 2). Core ELA6 (NH) has a radiocarbon age of 2064 ± 33 a BP (168 cal BCE to 18 cal CE) at 11.2 m bsl (Table 2). Other cores (ELA2 and ELA4, NH; and ELA9, SH) show calibrated ages up to the 2nd century CE for sediments near the bottom of their sedimentary sequence.

The absence of sediments older than 3 ka BP suggests that the harbour was probably dredged during the Roman period or more recent historical times. Dredging in antiquity is well documented in other Mediterranean areas (Marriner and Morhange, 2006b; Morhange and Marriner, 2010; Lisé-Pronovost et al., 2019), and many ancient ports were refashioned during the Roman period (e.g. Marriner et al., 2014). Eustacy must also be considered, given the early Holocene sea level rise of around 50–60 m recorded throughout the Mediterranean (Benjamin et al., 2017). Specifically, the estimated relative sea level (RSL) and shoreline predictions for the Levantine Mediterranean indicate that the shoreline in the study area was approximately −3.0 m at 6 ka BP and −0.25 m at 2 ka BP relative to the present shoreline (Lambeck and Purcell, 2005). According to Marriner et al. (2014), Levantine coastal harbours show a sequence starting with Early Holocene brackish water palaeoenvironments that mark sea level rise followed by shallow marine palaeoenvironments influenced by human activities. However, Alexandria port (Egypt) lacks typical Holocene lagoon palaeoenvironments beneath the transgressive sequence (Bernasconi et al., 2006). Although the Elaiussa Sebaste area is considered to have been tectonically quite stable in the late Holocene, except for recent uplifts highlighted by Desruelles et al. (2009) and Cosentino et al. (2016), the high seismicity of the southern part of Turkey must be considered (Ambraseys, 2009; Anzidei et al., 2011 and references therein). Late Quaternary tectonic activity, which uplifted these coastal areas and prevented sea intrusion until more recent times, could partly explain the absence of sediments older than 3 ka BP. Dredging activity, together with the natural process of uplift, could therefore explain the absence of sediments older than those found in the cores.

In the study area, most sediments are predominantly sandy with varying amounts of mud, reflecting conditions of higher and lower hydrodynamics. These deposits vary based on proximity to the open sea, with higher energy closer and lower energy further away, influenced by currents and waves. The superficial sands are yellowish, probably from aeolian material (Ballirano et al., 2003), and are overlaid by red soils ('*terre rosse*') used for farming in recent times (Fig. 2). All the cores contain darker muddy levels often rich in plant remains and charcoal. Pottery fragments (mainly amphorae shards) were found particularly in ELA7 (seaward sector near the Agora and Basilica) and ELA9 (SH). The Late Hellenistic pottery remains in core ELA7, at 7.3–8.2 m bsl, are contained in sediments dated to 150–70 BCE, testifying to human activity from the 2nd century BCE, as already supported by archaeological research. Relevant archaeological remains were not found in cores ELA2 (northernmost) and ELA4 (central NH).

Rich and diverse foraminiferal assemblages were consistently found in the sediments. Most are typical of modern Mediterranean coastal environments (brackish water, shoreface and vegetated shallow marine habitats), indicating well-established marine/brackish conditions in both harbours. The four recognized FAs represent different palaeoecological conditions of the harbours, varying from brackish water influence, protected settings, infralittoral vegetated and shallow coastal environments (Table 3).

The ostracod fauna in the cores is consistently present across all levels, primarily representing shallow coastal or partially protected environments with variable salinity values. PCA identified four main components (OAs) reflecting significant environmental changes over time in the NH area, which correlate with phases of growth or decline of port activity.

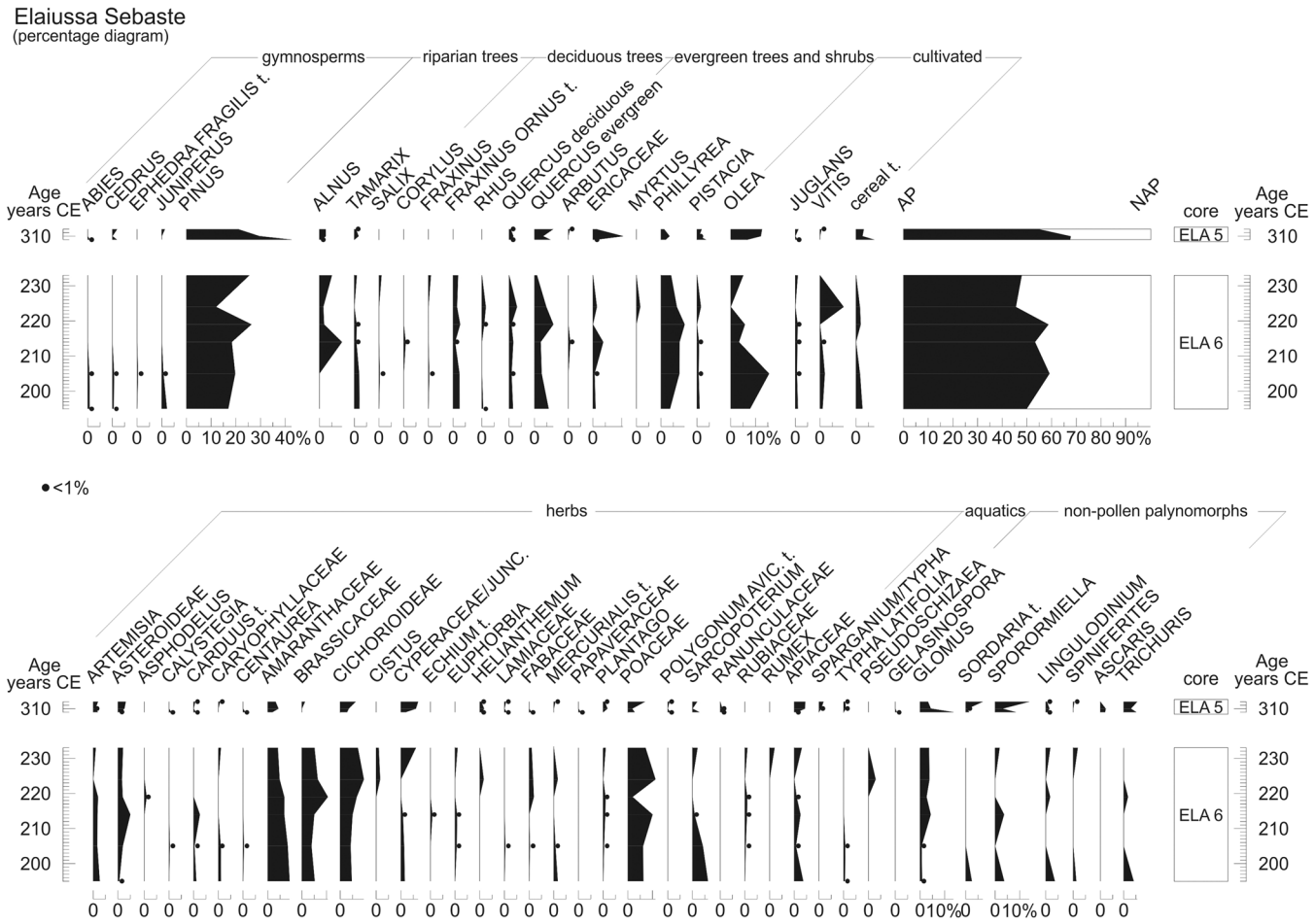

Figure 6. Pollen percentage diagram of cores ELA5 and ELA6 from Elaiussa Sebaste.

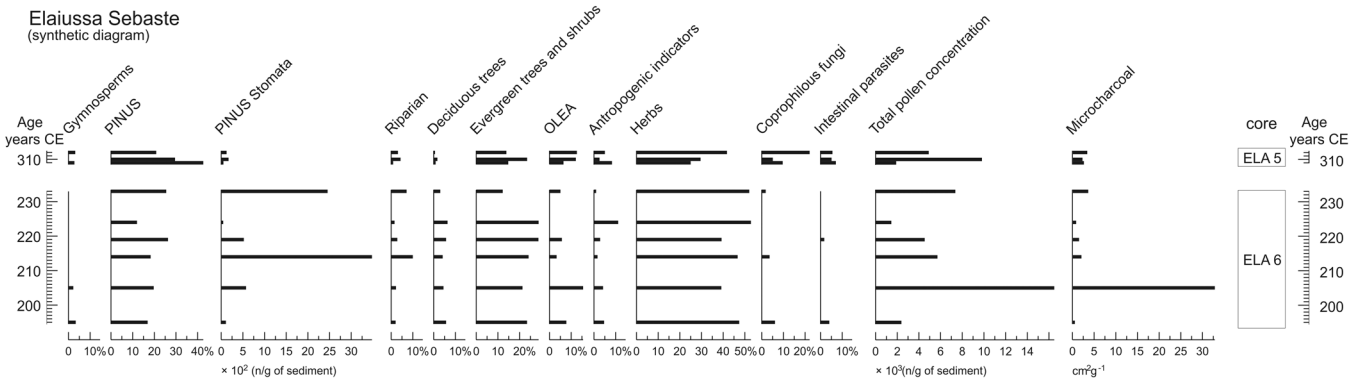

Figure 7. Summary pollen diagram including the cumulative percentages of gymnosperms, riparian trees, deciduous trees, evergreen trees and shrubs, anthropogenic indicators, herbs, coprophilous fungi, intestinal parasites, *Olea* and *Pinus* pollen percentages, stomata of *Pinus*, total pollen concentrations and microcharcoal concentrations.

The pollen data are consistent with the environmental conditions highlighted by micropalaeontological records. Pollen grains and NPPs of lagoons and shallow coastal basins, accompanied by other palynomorphs of freshwater environments, confirm a marked salinity variability.

Environmental interpretation of the Elaiussa Sebaste harbours, historical and archaeological implications

PCA of foraminiferal and ostracod associations from the NH and SH sedimentary series identified four main components (FAs and OAs) distinguishing different phases of environmental evolution from the 8th century BCE to the Early Byzantine periods. Pollen analysis results further defined environmental changes and land use activities during the Roman Imperial and Early Byzantine periods. Using Bayesian age–depth models (cores ELA5, ELA6 and ELA7, Fig. S1) and radiocarbon ages along with the other proxies, the environmental/historical evolution and associated human activities in the NH and SH of Elaiussa Sebaste have been reconstructed as follows.

Eighth century BCE to Late Hellenistic phase (790–30 BCE)

Sediments from this long time span were only found in the NH coastal area near the Agora, the Great Baths and the Theatre

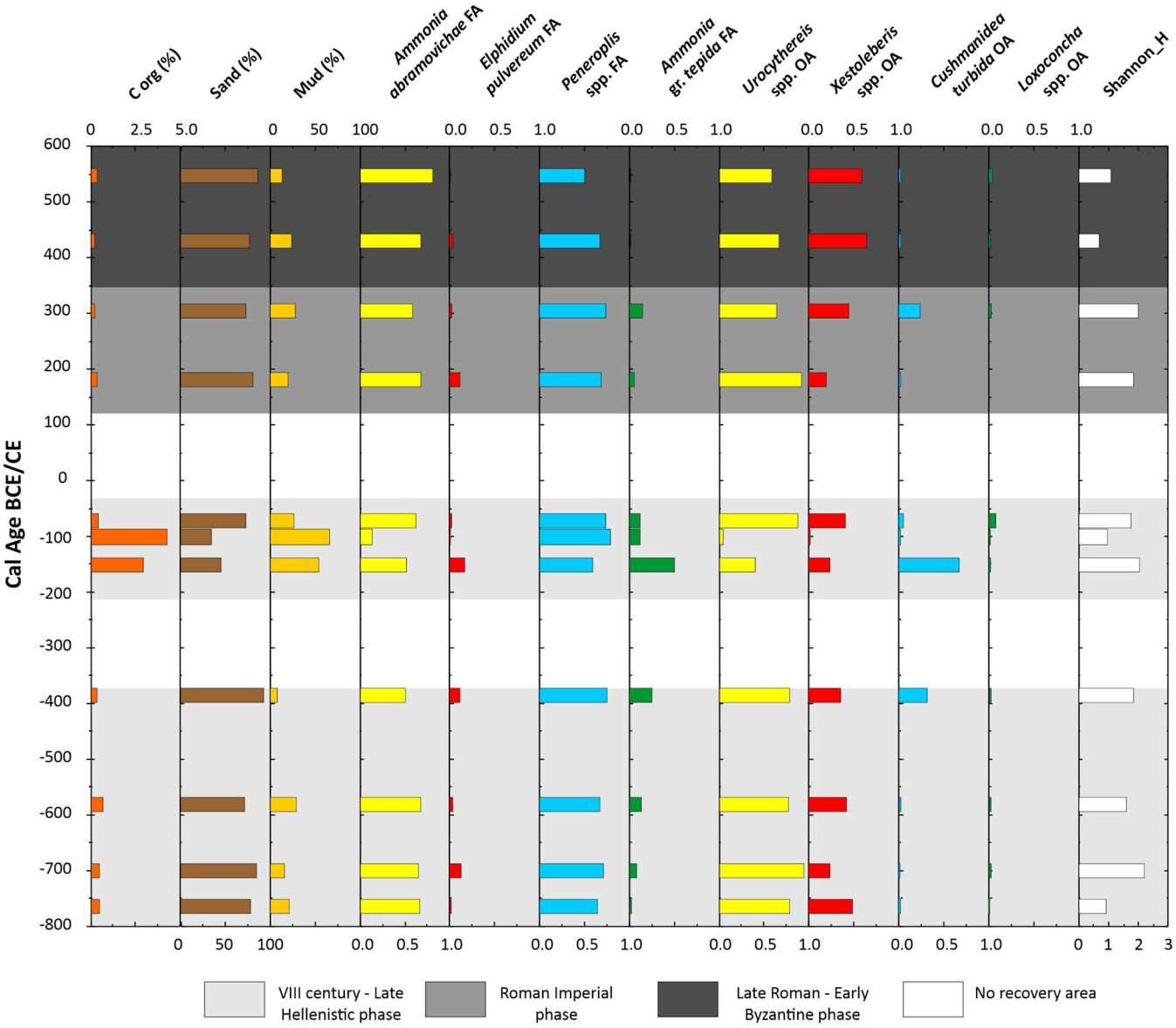

Figure 8. Vertical bar plot distribution versus calibrated ages (BCE/CE) of the geochemical (C_{org} %) and sedimentological (sand, mud %) features over core ELA7. Historical phase based on PCAs of foraminifera assemblages (FA) and ostracod assemblages (OA) is represented by light, medium and dark grey coloured bands. White bands represent intervals where sediment could not be recovered. Shannon index (H) for the ostracods is also reported. [Color figure can be viewed at wileyonlinelibrary.com]

(core ELA7, Fig. 1). These include sandy sediments from the 8th century BCE (Fig. S1), with low organic matter accumulation (C_{org} < 1%, Fig. 8). In these sediments, the *Peneroplis pertusus* FA and *Ammonia abramovichae* FA, subordinately, suggest infralittoral, vegetated marine bay environments with some hydrodynamics (Fig. 8; Table 3). Ostracods, mainly the *Urocythereis* spp. OA, also indicate a coastal vegetated environment (Fig. 8; Table 3).

The coastal sector in front of the Byzantine Palace is another area that records sediment from the Hellenistic period (ELA6, Fig. 1). Here, the oldest sediments, probably dating back to the 2nd century BCE (Fig. S2), are about 50 cm thick, deposited directly on the calcareous bedrock (Fig. 2). These silty sands indicate high hydrodynamics as suggested by the *A. abramovichae* FA (Fig. 9). The absence of older sediments comparable to those at the base of core ELA7 might be due to dredging in the NH's central sector. Foraminiferal and ostracod associations suggest that anthropogenic harbour activity had not yet begun. The Hellenistic period could refer to the proto-port phase or a pocket beach, in agreement with Marriner & Morhange (2007) (Fig. 10a).

This period is followed in the coastal sector of ELA7 core by finer sediments enriched in organic matter (C_{org} ≥ 3.0%) of continental origin (C/N > 10, Table S1). These sediments, dated to the 2nd to mid-1st century BCE (7.6–8 m bsl in ELA7; Figs. 2 and 8), are rich in charcoal and numerous Hellenistic ceramic fragments. During this period, a change in the ostracod association and a dramatic decline in the Shannon index (H < 1, Table S3) are observed. Foraminifera such as the *Ammonia* gr. *tepida* FA suggest a brackish environment with freshwater contributions near the isthmus (core ELA7), also supported by the presence of the *Cushmanidea turbida* OA, which tolerates salinity variations and trophic gradients (Mazzini et al., 2022 and references therein) (Table 3).

This swamping phase may reflect a more hydrodynamically protected environment, potentially linked to the early stages of port use. Historical sources indicate that port activity began at Elaiussa during this period, though evidence from ancient literary and numismatic sources is minimal (Equini Schneider, 1999; Tempesta et al., 2020).

Roman Imperial phase (30 BCE to 4th century CE)

The evolution of harbour activities during the Roman period (30 BCE to 350 CE) is well represented by the evolution of

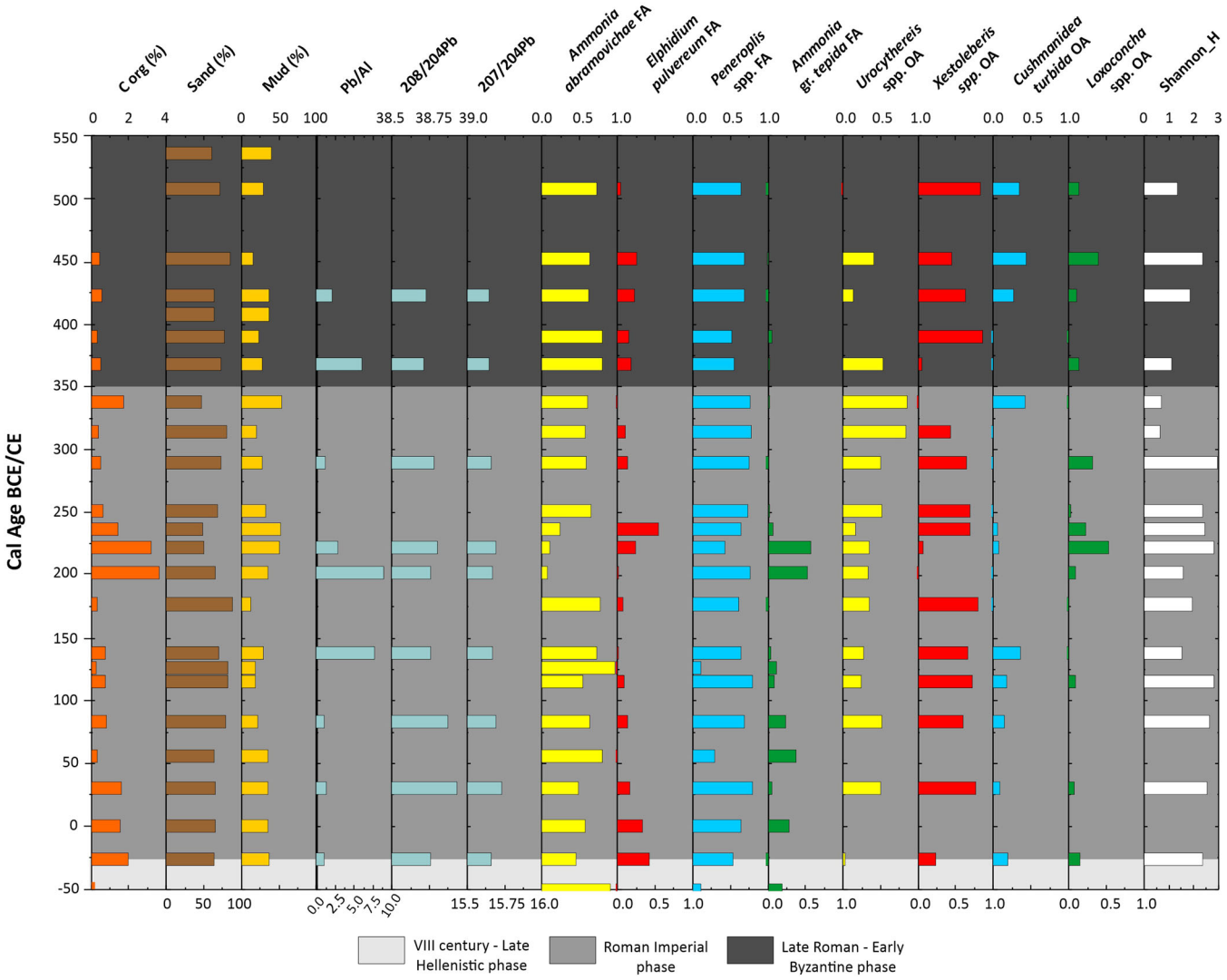

Figure 9. Vertical bar plot distribution versus calibrated ages (BCE/CE) of the geochemical (C_{org} %, Pb/Al, $^{208/204}$Pb and $^{207/204}$Pb) and sedimentological (sand, mud %) features over core ELA6. Historical phases based on PCAs of foraminifera assemblages (FA) and ostracod assemblages (OA) are represented by light, medium and dark grey coloured bands. Shannon index (H) for the ostracods is also reported. [Color figure can be viewed at wileyonlinelibrary.com]

foraminifer and ostracod associations. In core ELA7, the *Urocythereis* spp. OA signalled an infralittoral vegetated environment mainly from 70 BCE to 180 CE (Fig. 8). The ostracod H index, after a drastic drop around 100 BCE, returns to values >1 until 300 CE, confirming environmental stability. Conversely, increased anthropogenic harbour activity is recorded in the central harbour area, with an enrichment of continental organic matter in the southern sector of the NH (ELA6) around 30 BCE to 30 CE (Fig. 9). An increase in the *Elphidium pulvereum* FA suggests a protected environment, statistically supported by the *Xestoleberis* spp. OA, which persists longer than the foraminifera (Fig. 9; Table 3). This assemblage, dominated by the genus *Xestoleberis*, indicates a 'lagoon environment' and suggests a more sheltered area, in agreement with Mazzini et al. (2022).

Following Marriner & Morhange (2007) and Marriner et al. (2014), this phase could represent the development of human use of the port (Fig. 10b). The increasing mud content in the sediments probably indicates enhanced basin protection and increased competence in harbour construction. This aligns with the increasing importance of Elaiussa during the age of Augustus, and in the early reign of Tiberius, facilitating the growth of commercial activities.

The NH develops towards a coarsening texture around 80–180 CE (ELA7, Fig. 8; and ELA6, Fig. 9), indicating building activity in the harbour areas near the isthmus and city quarters. Elaiussa's new development began when Vespasian created the unified province of Cilicia in 72 CE and continued uninterrupted until the Severan age.

The sediments from this period have a sand content of >70%, with a general decrease in silt content. Foraminifera, represented by the *A. abramovichae* FA and *P. pertusus* FA (Figs. 8 and 9), indicate marine, sometimes vegetated (*P. pertusus* FA) environments. Conversely, ostracods suggest more variable salinity conditions, as indicated by the *Xestoleberis* spp. OA distribution (Fig. 9), in agreement with Mazzini et al. (2022). These species typically occupy sheltered areas where few can survive, indicating a challenging environment (Ruiz et al., 2000, 2006; Salvi et al., 2015, 2020). The presence of *Xestoleberis* spp. suggests ongoing human use of the bay, with the strong variability in ostracod H index values indicating substantial harbour activity.

Similarly, the sediments at the base of core ELA9 in the SH (Fig. 1) also indicate an age around 170 CE (Fig. 2). The dominant foraminifera association at the base suggests a vegetated infralittoral environment (*P. pertusus* FA), transitioning to a marine environment with some hydrodynamics toward the top (*A. abramovichae* FA) (Fig. S2). Numerous pottery fragments are found in these sediments. Unfortunately, the most superficial sediments of ELA9 have not been dated,

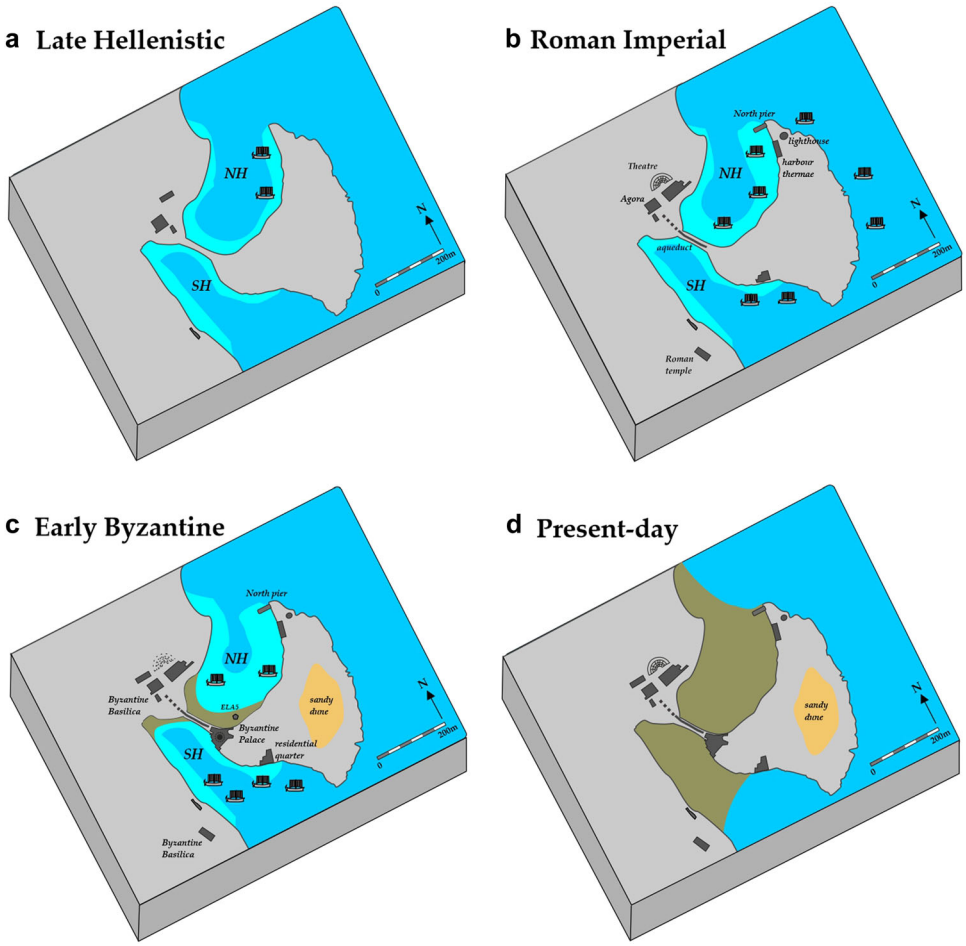

Figure 10. Overview of the palaeoenvironmental evolution of the studied area. The main phases treated in the Discussion are shown: (a) Late Hellenistic phase (790–30 BCE), (b) Roman Imperial phase (30 BCE to 4th century CE), (c) Late Roman to Early Byzantine phase (4th–7th century CE) and (d) present-day situation. The light blue colour indicates more coastal seabed, whereas the darker blue colour indicates deeper seabed. The green shading in (c) and (d) reflects the transition from marine to continental palaeoenvironments. [Color figure can be viewed at wileyonlinelibrary.com]

making it difficult to determine their historical period. However, it can be inferred that the SH was never well protected and was mainly used as a mooring area (Toro and Di Filippo, 1999; Tempesta et al., 2020).

Around 200–240 CE, both in the central NH (ELA6, Fig. 9) and near the entrance of the basin (ELA2, around 10 m bsl), an increase in mud and organic carbon (of continental origin, C/N > 10) is recorded. During this period, the *E. pulvereum* FA (notably in ELA2, Fig. S2) and *Ammonia* gr. *tepida* FA followed by the *E. pulvereum* FA (ELA6, Fig. 9) reached their peak significance, suggesting protected bay environments with significant low-salinity water influence.

Above 230 CE in core ELA6, ostracod associations are still mainly dominated by the *Xestoleberis* spp. OA, except for the *Loxoconcha* spp. OA, which became prevalent around 220 CE (Fig. 9). Both OA factors suggest shallow protected environments connected to the sea with high input of organic materials. Following Melis et al. (2015), this interval is interpreted as a phase of intense port activity, also marked by high local agricultural practices, as indicated by the pollen data and archaeological evidence.

Although the pollen record of ELA6 covers a short period (195–233 CE, Fig. 6), it provides insights into the land use of Elaiussa. Cereals, *Vitis*, *Olea* and *Juglans* were probably the main cultivated plants. Although wild olive plants grew in natural maquis, archaeological evidence confirms local cultivation and trade of olive oil (Equini Schneider, 1999; Efe et al., 2011; Ferrazzoli, 2013). The high frequencies of Brassicaceae may be partly related to cultivation, as documented in other sites of the Mediterranean during the Roman Imperial Period (Russo Ermolli et al., 2014; Vignola et al., 2022).

The pollen record also shows clear evidence of human impact on natural forest ecosystems. Intense pine forest clearance, confirmed by both the high concentration of stomata and presence of wood fragments of *Pinus* deposited within the sediment of the harbour (Figs. 6 and 7), favoured the development of evergreen shrubland formations (Fig. 6). Pines might have been a valuable resource as raw material and/or pitch source for local shipyards. Opening of the forest allowed the development of herbaceous formations typical of disturbed and degraded lands. The thorny bush *Sarcopoterium spinosum* dominated areas where the maquis failed to regenerate due to the long-term effects of anthropogenic pressure (Zohary, 1962). The occurrences of *Plantago*, *Rumex*, Fabaceae, Rubiaceae, *Echium*, *Centaurea* and *Asphodelus* suggest meadows disturbed by agricultural activities. *Sporormiella* and *Sordaria* point to the presence of herbivores related to livestock farming, while the continuous record of *Glomus* suggests soil erosion and downwash into the port.

The record of Amaranthaceae, and dinocysts of *Spiniferites* and *Lingulodinium*, as in other Mediterranean coastal environments (Di Rita et al., 2018, 2022) (Fig. 6), confirm the saline conditions of the harbour documented by the micropalaeontological analyses. However, the presence of *Psedoschizaea*, an algal spore associated with freshwater flows and erosional processes (Pantaléon-Cano et al., 2003), also suggests an input of erosive freshwater from the hinterland. This process might have slightly decreased the salinity of some parts of the

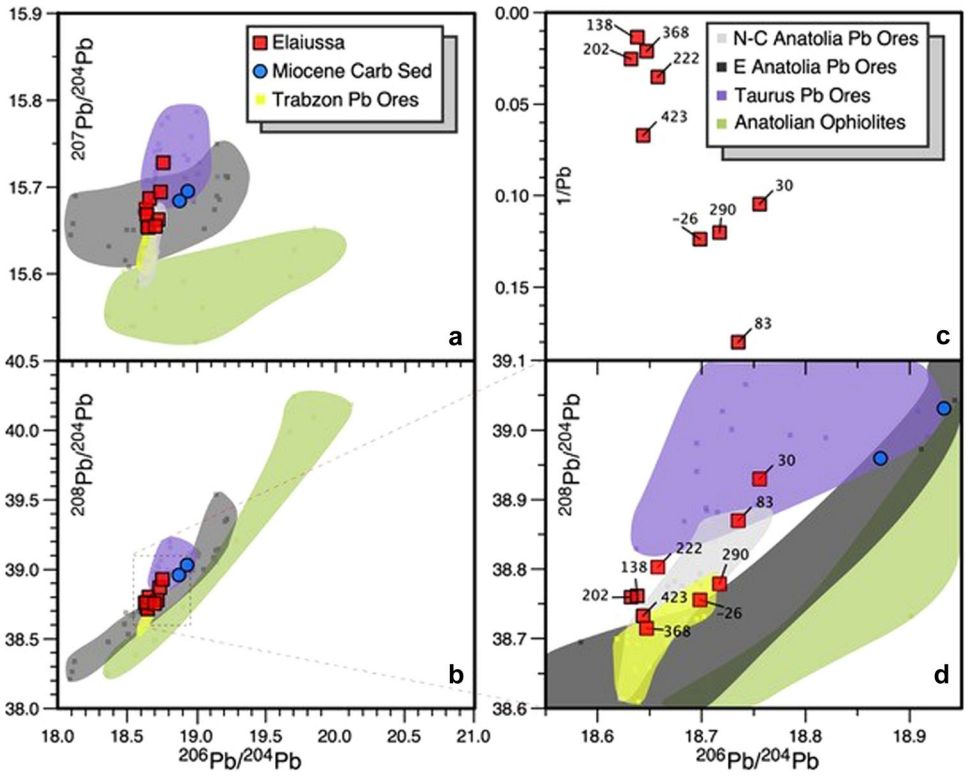

Figure 11. Diagram of $^{206}Pb/^{204}Pb$ isotope ratio vs. $^{207}Pb/^{204}Pb$ (a), $^{208}Pb/^{204}Pb$ (b, d) and Pb content, expressed as 1/Pb (c, [Pb] values expressed a $\mu g\ g^{-1}$). Boxed area in (b) is enlarged in (d) to highlight variations observed in studied samples. Labels in (c) and (d) represent sample age BCE (minus numbers) and CE. Pb isotope ratios of surrounding host rocks and of Anatolian Pb ores are plotted for comparison (data from: Klaver et al., 2015; Sayre et al., 2001; Çelik et al., 2013, De Ceuster & Degryse, 2023). [Color figure can be viewed at wileyonlinelibrary.com]

harbour, allowing the development of scattered aquatic vegetation formations composed of *Typha* and Cyperaceae. *Trichuris*, a helminth genus including intestinal parasites of humans and animals, might also indicate the influx of wastewater from the city (Fig. 6).

In the ELA6 (NH) core, a marked change in Pb concentration and Pb isotope composition is observed during 140–220 CE (Fig. 9). The Pb concentration suddenly increased from 5.6 to 74.4 ppm (Table S4) and the Pb/Al ratio rose from 1.0 to 8.9 (Fig. 9). Pb concentrations below 10 ppm and Pb/Al (EF) ratio below 3 usually indicate uncontaminated crustal sediments (see Véron et al., 2013), while higher values suggest contamination from anthropogenic metallurgical activity.

To differentiate geogenic from anthropogenic Pb sources, Pb isotopes of the samples are plotted with probable natural background and possible anthropic contaminants (Fig. 11). Surrounding rocks mostly belong to Middle Miocene carbonate sedimentary units or older ophiolitic melange (e.g. Şafak et al., 2005). These sources are represented in Fig. 11 by the Pb isotope data from two middle Miocene carbonate sediments dredged offshore (ODP/DSDP site 375; Klaver et al., 2015), which are the best representatives of the average sedimentary rock of the region, and Mesozoic ophiolites (after Çelik et al., 2013). Other local Pb sources, from rock weathering or local manufacturing, include Pb ores from the Taurus range, while external anthropogenic sources include Pb ores of Eastern Anatolia and North–Central Anatolia, and the Black Sea (Trabzon) region (data from Sayre et al., 2001; De Ceuster and Degryse, 2023).

The increased lead accumulation is probably related to its use in ships and sewage pipes during the Roman period (e.g. Delile et al., 2017). This might explain the presence of *Trichuris* eggs carried by faeces, but also the loading of *Pinus* waste, since metallurgy and mining depended on wood resources in historical times (Py et al., 2014; Di Rita et al., 2022, Silva-Sánchez & Armada, 2023). A microcharcoal peak may reflect the use of fire for both metallurgical and agrisilvicultural practices, as well as for shipbuilding activities (Fig. 7).

Several studies demonstrate Pb pollution during the Greek and Roman periods (Marriner & Morhange, 2007; Stock et al., 2013, Delile et al., 2017). Pb concentration doubled in Alexandria's harbour sediments during the Roman apogee (Véron et al., 2006) and increased more than tenfold over Greek sediments in Marseille's harbour (Le Roux et al., 2005). With the increase in Pb, the Pb isotopes $^{206/204}Pb$, $^{207/204}Pb$ and $^{208/204}Pb$ also similarly decrease with core depth (Fig. 9). The correlation between $^{206}Pb/^{204}Pb$ and 1/Pb (Fig. 11c) suggests that the isotope ratio changes align with Pb contamination, as inferred by Fagel et al. (2017), with a rough linear trend typical of mixing of sources in this kind of diagram. Elaiussa samples show a shift from typical local Pb isotope values (i.e. Miocene carbonates and local Pb ores) to those from external sources, probably from Trabzon, indicating contamination due to manufacturing (Fig. 11a, b). The $^{208}Pb/^{204}Pb$ vs. $^{206}Pb/^{204}Pb$ diagram (Fig. 11d) shows that the samples from 26 BCE to 83 CE and 290 CE have values typical of natural or local Pb coming from ores. Conversely, Pb isotope ratios of samples from the Roman Imperial period (138, 202 and 222 CE) and some from 368 and 423 CE (Byzantine period) show an external Pb influence due to human activity. This shift in Pb isotope ratios is also reflected in Pb contents. Samples with a local Pb fingerprint have low Pb concentrations (1/Pb > 0.1, Pb < 10 ppm), while those with a Trabzon-like Pb signature show significantly higher Pb concentrations.

A strong decrease in the $^{206}Pb/^{207}Pb$ ratio was also highlighted by Véron et al. (2013) in the port of Alexandria during the Roman period, around a calibrated age of 100–200 CE. Furthermore, the Pb isotope signal is useful for tracing metallurgy history and recording human activities to the origin of metal used

for artefacts (e.g. Sayre et al., 2001; Le Roux et al., 2005; Véron et al., 2006; Fagel et al., 2017; Di Rita et al., 2022).

Palaeoenvironmental indicators and isotopic geochemistry suggest the maximum activity of the NH occurred during this time, indicating the Roman harbour apogee, in agreement with Marriner & Morhange (2007) and Marriner et al. (2014) (Fig. 10b). This is consistent with the Ancient Harbour Facies (AHF) described by Marriner & Morhange (2006a, 2007). The decrease in texture of the sediment suggests a protected harbour environment with significant anthropic presence, testified by a high accumulation of organic matter of continental origin. This aligns with historical sources indicating the development of the city during the middle Roman imperial period. Monumental complexes such as the Theatre, Agora, Great Baths, Harbour Baths, Small Baths and Necropolis (Fig. 1) belong to this historical era. Additionally, the period around the 3rd century CE coincides with the 'Roman Climatic Optimum' (Margaritelli et al., 2020 and references therein).

A high sedimentation rate, reaching 4.1 cm a^{-1}, is observed in the northern NH from 230 CE (ELA2, Fig. 2) with sediments enriched in sand, especially in the middle sequence of the core (Fig. 5). The dominance of *A. abramovichae* and *Peneroplis* spp. FAs indicates open bay conditions (Fig. S2) though low-salinity influences are noted at about 10 m (230 CE) and 8 m bsl, as evidenced by the *Ammonia* gr. *tepida* FA (Fig. S2). Similarly, the *Urocythereis* spp. OA at 230 CE and the overlying *Xestoleberis* spp. OA highlight distinct environmental and anthropogenic activities in the outer harbour area. The ostracod H index mostly remains above 2 (Table S3). It is evident that the northernmost sector of the NH was more prone to siltation, accumulating about 9 m of sediment in 220 years due to its location near the harbour entrance where an *opus caementicium* pier was built near the limestone promontory to protect the harbour (Fig. 10b).

Late Roman to Early Byzantine phase (4th–7th century CE)

In the NH, a new phase of swamping occurred between about 300 and 400 CE, especially in the central (ELA3, ELA4, Fig. 2) and coastal (ELA5, Fig. 12) sectors. The sediments show increased mud and C_{org} (>1.0%) contents with the *E. pulvereum* FA (ELA3 and 5) and *Ammonia* gr. *tepida* FA (specifically for ELA4) indicating salinity variation and

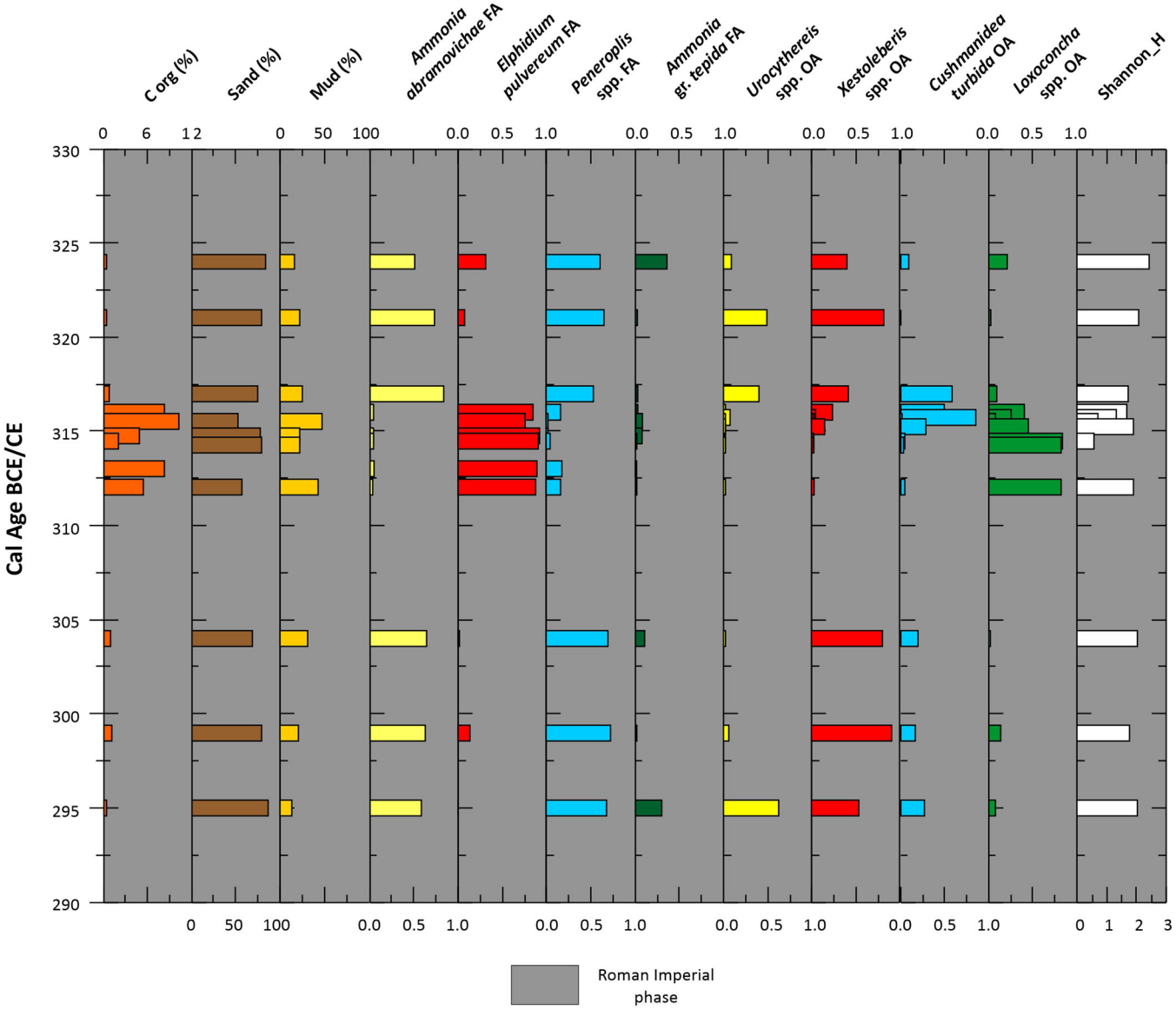

Figure 12. Vertical bar plot distribution versus calibrated ages (BCE/CE) of the geochemical (C_{org} %) and sedimentological (sand, mud %) features over core ELA7. The historical phase based on PCAs of foraminifera assemblages (FA) and ostracod assemblages (OA) is represented by the medium grey coloured band. Shannon index (H) for the ostracods is also reported. [Color figure can be viewed at wileyonlinelibrary.com]

renewed harbour protection. A new Pb/Al peak around 370 CE in core ELA6 indicates that the port remained active (Fig. 9).

More specifically, the coastal sector of the NH (ELA5) attests to a brief period with highly laminated sediments rich in charcoal and pollen, possibly indicating a change in agricultural activities. In this highly coastal sector (ELA5), ostracods record significant environmental changes in a protected setting with high variability in environmental parameters (specifically freshwater inputs) and high organic material accumulation, represented by the *Loxoconcha* spp. OA (Fig. 12). The sharp decline in the ostracod H index suggests probable environmental degradation in this bay, probably due to human activities.

Compared to core ELA6, the pollen record of ELA5 highlights a clear decline of vineyards and an intensification of cereal and olive cultivation in the 4th century CE (around 309–312 CE) (Figs. 6 and 7). The increase in *Ascaris* and *Trichuris* suggests increased wastewater influx into the harbour. The occurrence of these intestinal parasites, evidenced in the Roman harbour of Ephesus, was used as evidence of canalization of sewerage pipes in the city (Stock et al., 2016). Canalization was also hypothesized at Elaia Bay to explain a phase with high concentrations of these two parasites (Shumilovskikh et al., 2016). The increase of *Sporormiella, Sordaria* and *Glomus* reflects an intensification of livestock raising coupled with significant soil erosion.

The vegetation conditions shown by the ELA5 record were similar to those depicted in ELA6. The only exceptions were an increase in Ericaceae and a contemporary decline of *Phillyrea*, suggesting a reorganization of the dominant taxa inside the maquis, and a further development of sedges and *Typha* stands, possibly due to an intensification of freshwater input into the harbour (Fig. 6).

During the Early Byzantine period, around the mid-5th century CE, significant constructions included numerous Christian Churches, a Residential Quarter and a large palace on the southern edge of the promontory, built over earlier Hellenistic and Roman structures. This suggests a new phase of significant activity, mainly including the SH (Tempesta et al., 2020) (Fig. 10c). Post-400 CE periods are mainly recorded in cores from the north-central NH (cores ELA2, 4, 6, 7 and presumably core ELA3, Fig. 2). The lack of sediments more recent than mid-4th century in core ELA5 may indicate a reduction in the harbour extension, possibly due to human filling in the coastal area where core ELA5 is located (Fig. 10c).

Variable palaeoenvironments between the open and protected bay are observed in the central and northernmost NH (ELA2) around 450 CE, with an increase in mud content (Fig. 5), although foraminifera (*A. abramovichae* FA, Fig. S2) and ostracods (*Urocythereis* spp. OA) suggest less protected environments.

Marine palaeoenvironments persisted in the central NH (ELA6 and 7) until the mid-6th century CE. A decrease in mud content and sediment coarsening indicate sedimentation in shallow water (Figs. 8 and 9). The marked increase in the *A. abramovichae* FA in cores ELA2, 3, 4, 6 and 7 (Figs. 8, 9 and S2) points to a more coastal, hydrodynamic and less 'anthropized' environment. The prevalence of the *Urocythereis* spp. and *Xestoleberis* spp. OAs in surface levels of cores ELA2, 6 and 7 suggests an ecological shift to a shallow marine environment (Mazzini et al., 2011, 2022 and references therein), indicating reduced anthropogenic activity. The transition to a coarser texture in the upper sedimentary sequence of NH cores (ELA3, 4, 6 and 7, Fig. 5) probably indicates the terminal natural burial of these harbour areas. The most superficial sediments in all cores exhibit a yellowish colour, with clasts tending to be rounded, typical of wind transport. On the other hand, a large sandy dune also occupies a significant portion of the rocky promontory dividing the two harbours (Fig. 10c, d). Ballirano et al. (2003) suggest that sediment accumulation from the northwest (the Limonlu area) may have contributed to its creation. Originally, this sediment probably filled the NH before forming the dune.

It appears that both the NH and certainly SH underwent silting, gradually reducing their water volume (Fig. 10c). With an estimated sedimentation rate of around 2 cm a^{-1}, the basin would have naturally silted up rapidly, a process probably exacerbated by the absence of dredging within the harbour. While no specific dates confirm this, anthropic factors (reduced use) and natural factors (sediment accumulation from currents and winds) probably contributed to the decline of these marine environments in the late 6th to early 7th century CE. Tectonic movements may have also played a role in the decline of the port. During the Early Byzantine Tectonic Paroxysm (EBTP, from mid-4th to mid-6th centuries CE), a series of uplift events linked to devastating earthquakes impacted the entire Levantine region (Pirazzoli et al., 1996). Notably, the great earthquake of 526 CE devastated Antioch and Seleucia Pieria (Ambraseys, 2009), located not far from Elaiussa Sebaste. It is therefore plausible that co-seismic events contributed to the decline of the port of Elaiussa.

From the 6th CE to early 7th century CE, Elaiussa Sebaste became one of the major production centres of Late Roman 1 amphoras, which transported wine (and possibly oil) throughout the Mediterranean. The discovery of some kilns producing these amphoras and large amount of ceramic waste (mainly from this type of amphora) around the SH highlight the scale of this production (Ferrazzoli and Ricci, 2007, 2010; Borgia and Iacomi, 2010). However, this period also saw a decline in large-scale urban-archaeological activities, with kilns occupying pre-existing public buildings or the Necropolis Area. Day-to-day activities continued across the city until the mid-7th century CE, when gradual abandonment began. Partial occupation persisted until around 630–660 CE. Later occupations in the 11th–13th centuries CE were not permanant, indicating that by then Elaiussa Sebaste was largely in ruins and had been completely, or almost completely, abandoned (Equini Schneider, 2010). The evolution of the area after the demise of port activities is graphically shown in Fig. 10(d), which illustrates the current configuration of the shoreline.

Conclusions

The extensive multidisciplinary study carried out on cores extracted from the ancient port environments of Elaiussa has yielded a comprehensive and detailed understanding of the evolution of palaeoenvironments over the past 3000 years, set within its rich historical context. The analyses unequivocally confirmed that the two studied sectors were both shallow marine environments intimately connected to the northern and southern ports of the city. The data from foraminifera, ostracods and pollen offer critical insights into the developmental trajectory of these harbour areas.

Notably, the NH exhibited a significantly higher potential for sediment accumulation, with bedrock depths exceeding 15 m. The sedimentary record, spanning from the 8th century BCE to the 6th century CE, captures the distinct phases of the harbour's evolution. This includes an initial stage during the late Hellenistic period, a flourishing peak in the Roman Imperial period and a marked shift towards siltation in the late Byzantine period.

The findings compellingly suggest that both the northern and southern harbours underwent substantial siltation during the last period, leading to a critical reduction in water volume. This

decline probably resulted from a combination of socioeconomic factors, including a lapse in port maintenance, compounded by natural sediment accumulation driven by environmental forces, even related to co-seismic events. Despite evidence of vibrant trade activity in Elaiussa Sebaste until the 7th century CE, it is plausible that commercial operations gradually transitioned to the SH basin, particularly for the transportation of wine (and potentially oil) across the Mediterranean. Nonetheless, daily activities persisted in all city sectors until the mid-7th century CE, after which Elaiussa began its gradual abandonment. Later settlements between the 11th and 13th centuries CE failed to establish permanent residency, marking the final chapter in the long and relevant history of the city.

Supporting information

Additional supporting information can be found in the online version of this article.

Table S1. Textural data of the studied sediments (sand, silt, clay %, mean size – Mz, sorting – Sort, skewness – Sk) following the Shepard classification, total organic carbon (C_{org}), total nitrogen (N_{tot}), and molar ratio C_{org}/N_{tot} (C/N).

Table S2. Relative abundance of the foraminifera as a percentage of each species with respect to the total assemblage present in each sample. Taxa are listed in alphabetical order. Number of species and total number of specimens are reported for each sample.

Table S3. Ostracod relative abundance as percentage of each species with respect to the total assemblage present in each sample reported for the analysed cores (ELA2, ELA5, ELA6, ELA7). Taxa are listed in alphabetical order. Number of specimens, species and Shannon index (H) are also reported.

Table S4. Al–Pb contents and Pb isotope ratios of selected samples from core ELA6. The Late Roman sedimentary interval spans the levels ELA6.13, 14 and 16, highlighted in light orange.

Plate S1. Scanning electron photomicrographs of some foraminifer species representative of the Elaiusse Sebaste palaeoenvironments. The scale bar (100 µm) is valid for all images. a – *Adelosina carinatastriata*, side view; b – *A. dubia*, side view; c – *A. longirostra*, side view; d – *Coscinospira hemprichii*, side view; e – *Cycloforina* sp.1, side view; f – *Cycloforina* sp.1, opposite side view; g – *C. contorta*, side view; h – *Massilina secans*, side view; i – *M. gualtieriana*, side view; j – *Miliolinella semicostata*, side view; k – *M. subrotunda*, side view; l – *Pseudotriloculina inflata*, side side; m – *P. rotunda*, side view; n – *Quinqueloculina berthelotiana*, side view; o – *Q. bosciana*, side view; p – *Q. disparilis*, side view; q – *Q. laevigata*, side view; r – *Q.* cf. *Q. lamarckiana*, side view; s – *Q. milletti*, side view; t – *Q. parvula*, side view; u – *Q. schlumbergeri*, side view; v – *Q. seminulum*, side view; w – *Q. variolata*, side view; x – *Siphonaperta agglutinans*, side view; y – *S. aspera*, side view; z – *S. dilatata*, side view.

Plate S2. Scanning electron photomicrographs of some foraminifer species representative of the Elaiusse Sebaste palaeoenvironments. The scale bar (100 µm) is valid for all iamges. a – *Spiroloculina angulosa*, side view; b – *S. antillarum*, side view; c – *S. corrugata*, side view; d – *S. ornata*, side view; e – *S. ornata* var. *tricarinata*, side view; f – *Triloculina bermudezi*, side view; g – *T. marioni*, side view; h – *T. rotunda*, side view; i – *T. plicata*, side view; j – *Lobatula lobatula*, side view; k – *Ammonia pawlowskii*, spiral view; l – *A. pawlowskii*, umbilical view; m – *A. abramovichae*, umbilical view; n – *A. abramovichae*, spiral view; o – *A. abramovichae*, umbilical view; p – *A.* gr. *tepida*, spiral view; q – *A.* gr. *tepida*, umbilical view; r – *Rosalina bradyi*, spiral view; s – *Discorbis vilardeboanus* spiral view; t – *Elphidium pulvereum*, side view; u – *E. advena*, side view; v – *Cribroelphidium poeyanum*, side view; w – *Elphidium crispum*, side view; x – *Haynesina depressula*, side view; y – *H. germanica*, side view.

Plate S3. Scanning electron photomicrographs of the dominant ostracod species in the ostracod assemblages (OAs) as calculated by PCA in the archaeological site of Elaiusse Sebaste. The scale bar (100 µm) is valid for all images. (1) *Urocythereis* cf. *britannica*, right valve; (2) *Aurila convexa*, left valve; (3) *Xestoleberis communis*, left valve; (4) *Xestoleberis dispar*, left valve; (5) *Xestoleberis plana*, left valve; (6) *Cistacythereis caelatura*, right valve; (7) *Cushmanidea turbida*, left valve; (8) *Loxoconcha rubritincta*, left valve; (9) *Loxoconcha stellifera*, right valve; (10) *Leptocythere levis*, right valve.

Figure S1. The Bayesian age-depth model for cores ELA5, ELA6 and ELA7 constructed using the software Bacon version 2.5.5.

Figure S2. Distribution of the Foraminiferal Association with the depth for the cores for which the age model could not be calculated. D1 = *Ammonia abramovichae* FA; D2 = *Elphidium pulvereum* FA; D3 = *Peneroplis* spp. FA; D4 = *Ammonia* gr. *tepida* FA.

Acknowledgments. Funding for this research was provided by the Italian PRIN 2009 project 'Studio geologico relativo all'evoluzione paleoambientale e paleoclimatica olocenica nell'area archeologica di Elaiussa Sebaste (Turchia sudorientale)' (scientific coordinators E. Equini Schneider and N. Pugliese). The authors gratefully acknowledge E. Equini Schneider for scientific and logistical assistance provided during the project, the Language Centre of the University of Trieste (CLA) for English language corrections, M. Crosera for geochemical analyses (Pb and Al), C. Landucci for C_{org} analyses and M. Braini for field assistance. Open access publishing facilitated by Universita degli Studi di Trieste, as part of the Wiley - CRUI-CARE agreement. We sincerely thank the editor and the two anonymous reviewers for their useful comments, which improved the paper.

Data availability statement

The data that support the findings of this study are available in the Supporting Information of this article.

Abbreviations. AHF, Ancient Harbour Facies; AMS, accelerator mass spectrometry; AP, arboreal pollen; BCE, before common era; BP, before present; CE, common era; C_{org}, total organic carbon; EBTP, Early Byzantine Tectonic Paroxysm; EF, crustal enrichment factor; ERT, electrical resistivity tomography; FAs, foraminiferal assemblages; FD, faunal density; GPR, ground penetrating radar; H, Shannon index; L, limestone bedrock; mls, modern mean sea level; m bsl, metres below the mean sea level altitude; NH, Northern Harbour; NPPs, non-pollen palynomorphs; N_{tot}, total nitrogen; OAs, ostracod assemblages; PCA, principal component analysis; PCs, principal component scores; RSL, estimated relative sea level; SH, Southern Harbour; Sort, sorting; WoRMS, World Register of Marine Species; WT, water table.

References

Aiello, G., Amato, V., Barra, D., Caporaso, L., Caruso, T., Giaccio, B. et al. (2020) Late Quaternary benthic foraminiferal and ostracod response to palaeoenvironmental changes in a Mediterranean coastal area, Port of Salerno, Tyrrhenian Sea. *Regional Studies in Marine Science*, 40, 101498. Available at: https://doi.org/10.1016/j.rsma.2020.101498

Aiello, G. & Barra, D. (2010) Crustacea, Ostracoda. *Biologia Marina Mediterranea*, 17(Suppl. 1), 401–419. Available at: https://doi.org/10.1093/oso/9780199233267.003.0025

Akkemik, Ü. & Yaman, B. (2012) *Wood anatomy of Eastern Mediterranean species*. Kessel Publishing House.

Albani, A.D., Favero, V. & Serandrei Barbero, R. (1991) The distribution and ecological significance of recent Foraminifera in the lagoon south of Venice (Italy). *Revista española de micropaleontología*, 23, 29–45.

Algan, O., Yalçın, M.N., Özdoğan, M., Yılmaz, Y., Sarı, E., Kırcı-Elmas, E. et al. (2011) Holocene coastal change in the ancient harbor of Yenikapı-İstanbul and its impact on cultural history. *Quaternary Research*, 76, 30–45.

Amato, V., Aiello, G., Barra, D., Caporaso, L., Caruso, T., Giaccio, B. et al. (2020) Holocene paleogeographic evolution of an ancient port city of the central Mediterranean area: natural and anthropogenic modifications from Salerno city, southern Italy. *Geoarchaeology*, 35(3), 366–383. Available at: https://doi.org/10.1002/gea.21774

Amato, V., Cicala, L., Valente, E., Ruello, M.R., Esposito, N. & Ermolli, E.R. (2021) Anthropogenic amplification of geomorphic processes along the Mediterranean coasts: a case-study from the Graeco-Roman town of Elea-Velia (Campania, Italy). *Geomorphology*, 383, 107694. Available at: https://doi.org/10.1016/j.geomorph.2021.107694

Ambraseys, N. (2009) *Earthquakes in the Mediterranean and Middle East: a multidisciplinary study of seismicity up to 1900*. Cambridge University Press. p. 947

Amorosi, A., Colalongo, M.L., Fiorini, F., Fusco, F., Pasini, G., Vaiani, S.C. et al. (2004) Palaeogeographic and palaeoclimatic evolution of the Po Plain from 150-ky core records. *Global and Planetary Change*, 40, 55–78.

Anzidei, M., Antonioli, F., Benini, A., Lambeck, K., Sivan, D., Serpelloni, E. et al. (2011) Sea-level change and vertical land movements since the last two millennia along the coasts of southwestern Turkey and Israel. *Quaternary International*, 232, 13–20.

Athersuch, J. (1979) The ecology and distribution of the littoral ostracods of Cyprus. *Journal of Natural History*, 13, 135–160.

Ballirano, P., Burragato, F., Di Filippo, M., Gaglianone, G., La Monica, G.B. & Landini, B. (2003) Caratteristiche tessiturali e provenienza delle sabbie nell'area di Elaiussa. In: Equini Schneider, E. (Ed.) *Elaiussa Sebaste II. Un porto tra Oriente e Occidente*. Roma, Italy: L'Erma di Bretschneider, pp. 764–771.

Barbanera, M. (2022) Elaiussa Sebaste: Relazione sulla campagna di scavo 2021. *Scienze dell'Antichità*, 28, 3–37.

Barbieri, G., Rossi, V., Vaiani, S.C. & Horton, B.P. (2019) Benthic ostracoda and foraminifera from the north Adriatic Sea (Italy, Mediterranean Sea): a proxy for the depositional characterisation of river-influenced shelves. *Marine Micropaleontology*, 153, 101772.

Benjamin, J., Rovere, A., Fontana, A., Furlani, S., Vacchi, M., Inglis, R.H. et al. (2017) Late Quaternary sea-level changes and early human societies in the central and eastern Mediterranean Basin: an interdisciplinary review. *Quaternary International*, 449(2017), 29–57. Available at: https://doi.org/10.1016/j.quaint.2017.06.025.

Bernasconi, M.P., Melis, R. & Stanley, J.D. (2006) Benthic biofacies to interpret Holocene environmental changes and human impact in Alexandria's Eastern Harbour, Egypt. *The Holocene*, 16, 1163–1176.

Bonaduce, G., Ciampo, G. & Masoli, M. (1976) Distribution of Ostracoda in the Adriatic Sea. *Pubblicazione della Stazione Zoologica di Napoli*, 40, 1–304.

Bonaduce, G., Masoli, M., Minichelli, G. & Pugliese, N. (1980) Some new benthic marine ostracod species from the Gulf of Aqaba (Red Sea). *Bollettino della Società Paleontologica Italiana*, 19, 143–178.

Borgia, E. & Iacomi, V. (2010) Note preliminari su un complesso industriale per la produzione di anfore Late Roman I a Elaiussa Sebaste (Cilicia). In: Milanese, M., Ruggeri, P., Vismara, C. (Eds.) *L'Africa Romana*. Atti del XVIII convegno di studio "I luoghi e le forme dei mestieri e della produzione nelle province africane", 1029–1053.

Breman, E. (1976) *The distribution of ostracodes in the bottom sediments of the Adriatic Sea*. Thesis, Free University of Amsterdam, Nederland, p. 165.

Carbonel, P. (1982) Les ostracodes, traceurs des variations dans des systèmes de transition eaux douces eaux salées. *Mémoire de la Société géologique de France*, 144, 17–128.

Çelik, Ö.F., Chiaradia, M., Marzoli, A., Billor, Z. & Marschik, R. (2013) The Eldivan ophiolite and volcanic rocks in the İzmir–Ankara–Erzincan suture zone, Northern Turkey: geochronology, whole-rock geochemical and Nd–Sr–Pb isotope characteristics. *Lithos*, 172–173, 31–46. Available at: https://doi.org/10.1016/j.lithos.2013.03.010

Cimerman, F. & Langer, M.R. (1991) Mediterranean Foraminifera. Slovenska Akademija Znanosti in Umetnosti. Academia Scientiarium et Artium Slovenica. Classis 4, *Historia Naturalis* 30, 118 pp.

Clark, R.L. (1982) Point count estimation of charcoal in pollen preparations and thin sections of sediments. *Pollen et Spores*, 24, 523–535.

Cosentino, D., Öğretmen, N., Cipollari, P., Gliozz, E., Radeff, G., Yıldırım, C. et al. (2016) Evidence for latest Pleistocene to Holocene uplift of the southern margin of the Central Anatolian Plateau (CAP), southern Turkey. EGU General Assembly 2016, *Geophysical Research Abstracts*, 18, EGU 2016–8873.

Cosentino, D., Schildgen, T.F., Cipollari, P., Faranda, C., Gliozzi, E., Hudackova, N. et al. (2012) Late Miocene surface uplift of the southern margin of the Central Anatolian Plateau, Central Taurides, Turkey. *Geological Society of America Bulletin*, 124(1/2), 133–145. Available at: https://doi.org/10.1130/B30466.1

Debenay, J.P., Guillou, J.J., Redois, F. & Geslin, E. (2000) Distribution trends of foraminiferal assemblages in paralic environments: a base for using foraminifera as bioindicators. In: Martin, R.E. (Ed.) *Environmental micropaleontology: The Application of Microfossils to Environmental Geology*. Kluwer Academic/Plenum Publishers, pp. 39–67.

De Ceuster, S. & Degryse, P. (2023) Dataset of lead isotope ratios of lead ores. Available at: https://doi.org/10.48804/D4DPLJ, KU Leuven RDR, V1.

Delile, H., Keenan-Jones, D., Blichert-Toft, J., Goiran, J.P., Arnaud-Godet, F. & Albarède, F. (2017) Rome's urban history inferred from Pb-contaminated waters trapped in its ancient harbor basins. *Proceedings of the National Academy of Sciences*, 114(38), 10059–10064.

Desruelles, S., Chabrol, A., Hasenohr, C., Pavlopoulos, K., Apostolopoulos, G., Kapsimalis, V. et al. (2023) Palaeogeographic reconstruction of the Main Harbour of the ancient city of Delos (Greece). *Journal of Archaeological Science*, 160, 105857. Available at: https://doi.org/10.1016/j.jas.2023.105857

Desruelles, S., Fouache, É., Ciner, A., Dalongeville, R., Pavlopoulos, K., Kosun, E. et al. (2009) Beachrocks and sea level changes since Middle Holocene: comparison between the insular group of Mykonos–Delos–Rhenia (Cyclades, Greece) and the southern coast of Turkey. *Global and Planetary Change*, 66(1–2), 19–33. Available at: https://doi.org/10.1016/j.gloplacha.2008.07.009

Di Donato, V., Ruello, M.R., Liuzza, V., Carsana, V., Giampaola, D., Di Vito, M.A. et al. (2018) Development and decline of the ancient harbor of Neapolis. *Geoarchaeology*, 33, 542–557. Available at: https://doi.org/10.1002/gea.21673

Di Filippo, M. & Toro, B. (2003) Prospezioni geofisiche a Elaiussa Sebaste. In: Equini Schneider, E. (Ed.) *Elaiussa Sebaste II. Un porto tra Oriente e Occidente*. Roma, Italy: L'Erma di Bretschneider, pp. 759–763.

Di Rita, F., Ghilardi, M., Fagel, N., Vacchi, M., Warichet, F., Delanghe, D. et al. (2022) Natural and anthropogenic dynamics of the coastal environment in northwestern Corsica (western Mediterranean) over the past six millennia. *Quaternary Science Reviews*, 278, 107372. Available at: https://doi.org/10.1016/j.quascirev.2022.107372

Di Rita, F., Molisso, F. & Sacchi, M. (2018) Late Holocene environmental dynamics, vegetation history, human impact, and climate change in the ancient Literna Palus (Lago Patria; Campania, Italy). *Review of Palaeobotany and Palynology*, 258, 48–61.

Donnici, S. & Serandrei Barbero, R. (2002) The benthic foraminiferal communities of the northern Adriatic continental shelf. *Marine Micropaleontology*, 44, 93–123.

D'Orefice, M., Bellotti, P., Bertini, A., Calderoni, G., Censi Neri, P., Di Bella, L. et al. (2020) Holocene evolution of the Burano Paleo-Lagoon (Southern Tuscany, Italy). *Water*, 12, 1007. Available at: https://doi.org/10.3390/w12041007

Efe, R. (2011) Olive and Olive Oil Culture in the Mediterranean Basin. In: Efe, R., Ozturk, M. & Ghazanfar, S., (Eds.) *Environment and Ecology in the Mediterranean Region*. Cambridge Scholars Publishing, UK, pp. 55–64.

El Baz, S.M. (2017) Recent Benthic Foraminifera as ecological indicators in Manzala Lagoon, Egypt. *Revue de Micropaléontologie*, 60, 435–447.

Elshanawany, R., Ibrahim, M.I., Milker, Y., Schmiedl, G., Badr, N., Kholeif, S.E.A. et al. (2011) Anthropogenic impact on benthic foraminifera, Abu-Qir Bay, Alexandria, Egypt. *The Journal of Foraminiferal Research*, 41, 326–348.

Equini Schneider, E. (1999) *Elaiussa Sebaste I. Campagne di scavo 1995–1997*. L'Erma di Bretschneider, Roma, Italy, p. 480.

Equini Schneider, E. (2003) *Elaiussa Sebaste II. Un porto tra Oriente e Occidente*. L'Erma di Bretschneider Roma, Italy, p. 383.

Equini Schneider, E. (2007) *Elaiussa Sebaste-Report of 2006 Excavation Season*, 29 Kazı Sonuçları Toplantısı, Kocaali, 299-310.

Equini Schneider, E. (2010) *Elaiussa Sebaste III. L'Agorà romana*. Turkey: Ege Yayinlari, p. 420

Faegri, K. & Iversen, J. (1989) *Textbook of Pollen Analysis*. Faegri K, Kaland PE, Krzywinski KJ (Eds.), Wiley and Sons, New York, p. 328.

Fagel, N., Lechenault, M., Fontaine, F., Pleuger, E., Otten, J., Allan, M. et al. (2017) Record of human activities in the Pb isotopes signatures of coastal sediments from the Roman archaeological site of Cala Francense, Cape Corsica (France). *Journal of Archaeological Science: Reports*, 12, 770–781.

Ferrazzoli, A.F. (2013) Production and Trade of a Cilician City from the Roman to Byzantine Age: The case of Elaiussa Sebaste. In: Hoff, M.C. & Townsend, R.F. (Eds.) *Rough Cilicia: New Historical and Archaeological Approaches*. Oxford: Oxford Books, pp. 210–218.

Ferrazzoli, A.F. & Ricci, M. (2007) Late roman 1 amphora types produced at Elaiussa Sebaste: archaeometrical analysis. In: Bonifay, M. & Treglia, J.C. (Eds.) *LRCW 2, Late Roman Coarse Wares, Cooking Wares and Amphorae in the Mediterranean*, Archaeology and Archaeometry, BAR Int. Ser.1662, Oxford, 689–700.

Ferrazzoli, A.F. & Ricci, M. (2010) Un centro di produzione delle anfore LR1: Elaiussa Sebaste in Cilicia (Turchia). Gli impianti, le anfore. *LRCW 3, Late Roman Coarse Wares, Cooking Wares and Amphorae in the Mediterranean, Archaeology and Archaeometry, Parma-Pisa 2008, BAR Int. Ser.* 2185, 815–826.

Folk, R.L. & Ward, W.C. (1957) Brazos River bar: a study in the significance of grain size parameters. *Journal of Sedimentary Research*, 27, 3–26.

Fouache, É., Sibella, P. & Dalongeville, R. (2005) Harbours and Holocene variations of the shoreline between Andriake and Alanya (Turkey). *Méditerranée*, 104, 87–94. Available at https://doi.org/10.4000/mediterranee.1432

Ghilardi, M. (2021) Geoarchaeology: Where geosciences meet the humanities to reconstruct past human–environment interactions. An application to the coastal areas of the Largest Mediterranean Islands. *Applied Sciences*, 11, 4480. Available at: https://doi.org/10.3390/app11104480

Giaime, M., Marriner, N., Morhange, C. (2019) Evolution of ancient harbours in deltaic contexts: a geoarchaeological typology. *Earth-Science Reviews*, 191, 141–167. Available at: https://doi.org/10.1016/j.earscirev.2019.01.022

Goñi, M.A., Teixeira, M.J. & Perkey, D.W. (2003) Sources and distribution of organic matter in a river dominated estuary (Winyah Bay, SC, USA). *Estuarine, Coastal and Shelf Science*, 57(5), 1023–1048.

Hayward, B.W., Holzmann, M., Pawlowski, J., Parker, J.H., Kaushik, T., Toyofuku, M.S. et al. (2021) Molecular and morphological taxonomy of living *Ammonia* and related taxa (Foraminifera) and their biogeography. *Micropaleontology*, 67(2-3), 109–274. Available at: https://doi.org/10.47894/mpal.67.3.01

Hedges, J.I. & Stern, J.H. (1984) Carbon and nitrogen determinations of carbonate containing solids. *Limnology and Oceanography*, 29, 657–663.

Jorissen, F.J. (1987) The distribution of benthic foraminifera in the Adriatic Sea. *Marine Micropaleontology*, 12, 21–48.

Kaniewski, D., Marriner, N., Sarti, G., Bertoni, D., Marchesini, M., Rossi, V. et al. (2022) Northern Adriatic environmental changes since 500 AD reconstructed at Aquileia (Italy). *Quaternary Science Reviews*, 287, 107565. Available at: https://doi.org/10.1016/j.quascirev.2022.107565

Kiliç, M. (2001) Recent ostracoda (Crustacea) fauna of the Black Sea coasts of Turkey. *Turkish Journal of Zoology*, 25, 375–388.

Kılıç, M., Altinsaçli, S., Balkis, H. & Balkis-Ozdelice, N. (2000) The ostracods species collected from coasts of The Gökçeada (Imbroz) Island (Aegean Sea). *Turkish Journal of Marine Sciences*, 6, 87–102.

Klaver, M., Djuly, T., de Graaf, S., Sakes, A., Wijbrans, J., Davies, G. et al. (2015) Temporal and spatial variations in provenance of Eastern Mediterranean Sea sediments: implications for Aegean and Aeolian arc volcanism. *Geochimica et Cosmochimica Acta*, 153, 149–168. Available at: https://doi.org/10.1016/j.gca.2015.01.007

Kubanç, C. (2003) Ostracoda (Crustacea) fauna of the Black Sea Coasts of Istanbul. *Turkish Journal of Marine Sciences*, 9, 147–162.

Külköylüoğlu, O., Colin, J.P., & Kiliç, M. (2005) New observations on live Loculicytheretta pavonia (Brady, 1866) (Ostracoda) from Turkey. *Crustaceana*, 78, 311–321.

Lambeck, K. & Purcell, A. (2005) Sea-level change in the Mediterranean Sea since the LGM: model predictions for tectonically stable areas. *Quaternary Science Reviews*, 24, 1969–1988.

Langlet, D., Baal, C., Geslin, E., Metzger, E., Zuschin, M., Riedel, B. et al. (2014) Foraminiferal species responses to in situ, experimentally induced anoxia in the Adriatic Sea. *Biogeosciences*, 11, 1775–1797. Available at: https://doi.org/10.5194/bg-11-1775-2014

Le Roux, G., Véron, A. & Morhange, C. (2005) Lead pollution in the ancient harbours of Marseilles. *Méditerranée. Revue géographique des pays méditerranéens/Journal of Mediterranean Geography*, 104, 31–35.

Lisé-Pronovost, A., Salomon, F., Goiran, J.-P., St-Onge, G., Herries, A.I.R., Montero-Serrano, J.C. et al. (2019) Dredging and canal gate technologies in Portus, the ancient harbour of Rome, reconstructed from event stratigraphy and multi-proxy sediment analysis. *Quaternary International*, 511, 78–93. Available at: https://doi.org/10.1016/j.quaint.2018.05.018

Margaritelli, G., Cacho, I., Català, A., Barra, M., Bellucci, L.G., Lubritto, C. et al. (2020) Persistent warm Mediterranean surface waters during the Roman period. *Scientific Reports*, 10, 10431. Available at: https://doi.org/10.1038/s41598-020-67281-2

Marriner, N. & Morhange, C. (2006a) The 'Ancient Harbour Parasequence': Anthropogenic forcing of the stratigraphic highstand record. *Sedimentary Geology*, 186, 13–17.

Marriner, N. & Morhange, C. (2006b) Geoarchaeological evidence for dredging in Tyre's ancient harbour, Levant. *Quaternary Research*, 65, 164–171.

Marriner, N. & Morhange, C. (2007) Geoscience of ancient Mediterranean harbours. *Earth-Science Reviews*, 80, 137–194.

Marriner, N., Morhange, C., Kaniewski, D. & Carayon, N. (2014) Ancient harbour infrastructure in the Levant: tracking the birth and rise of new forms of anthropogenic pressure. *Scientific Reports*, 4, 5554. Available at: https://doi.org/10.1038/srep05554

Mazzini, I., Aiello, G., Frenzel, P. & Pint, A. (2022) Marine and marginal marine Ostracoda as proxies in geoarchaeology. *Marine Micropaleontology*, 174, 102054. Available at: https://doi.org/10.1016/j.marmicro.2021.102054

Mazzini, I., Faranda, C., Giardini, M., Giraudi, C. & Sadori, L. (2011) Late Holocene palaeoenvironmental evolution of the Roman harbour of Portus, Italy. *Journal of Paleolimnology*, 46, 243–256. Available at: https://doi.org/10.1007/s10933-011-9536-7

McLennan, S.M. (1995) Sediments and soils: chemistry and abundances. In: *Rock physics and phase relations, A handbook of physical constants, AGU Reference Shelf*, 3, 8-19.

Melis, R., Bernasconi, M.P., Colizza, E., Di Rita, F., Equini Schneider, E., Forte, E. et al. (2015) Late Holocene palaeoenvironmental evolution of the northern harbour at the Elaiussa Sebaste archaeological site (South-Eastern Turkey): evidence from core ELA6. *Turkish Journal of Earth Sciences*, 24(6), 566–584. Available at: https://doi.org/10.3906/yer-1504-10

Melis, R. & Covelli, S. (2013) Distribution and morphological abnormalities of recent foraminifera in the Marano and Grado Lagoon (North Adriatic Sea, Italy). *Mediterranean Marine Science*, 14, 432–450.

Melis, R. & Violanti, D. (2006) Foraminiferal biodiversity and Holocene evolution of the Phetchaburi coastal area (Thailand Gulf). *Marine Micropaleontology*, 61, 94–115.

Meric, E., Avsar, N., Nazik, A., Yokes, M.B. & Dincer, F. (2008) A review of benthic foraminifers and ostracodes of the Antalya coast. *Micropaleontology*, 54, 199–240.

Meric, E., Avsar, N., Yokes, M.B. & Dincer, F. (2014) Atlas of Recent Benthic foraminifera from Turkey. *Micropaleontology*, 60, 211–398.

Meriç, E., Avşar, N. & Bergin, F. (2004) Benthic Foraminifera of Eastern Aegean Sea (Turkey) Systematics vs Autoecology. *Istanbul, Turkish Marine Research Foundation*, 18, 1–306.

Milker, Y. & Schmiedl, G. (2012) A taxonomic guide to modern benthic shelf foraminifera of the western Mediterranean Sea. *Palaeontologia Electronica*, 15, 134.

Morhange, C. & Marriner, N. (2010) Mind the (stratigraphic) gap: roman dredging in ancient Mediterranean harbours. *Bollettino di Archeologia on line*, 1, 23–32.

Morhange, C., Marriner, N. & Carayon, N. (2015) The geoarchaeology of ancient Mediterranean harbours. In: Arnaud-Fassetta, G. &

Carcaud, N. (Eds.) *French geoarchaeology in the 21st century*. Paris: CNRS editions, Alpha, pp. 281–289.
Morhange, C., Marriner, N. & Carayon, N. (2016) Eco-history of ancient Mediterranean harbours. In: Bekker-Nielsen, T. & Gertwagen, R. (Eds.) *The inland seas, towards an ecohistory of the Mediterranean and the Black Sea*. Stuttgard: Franz Steiner, Verlag, pp. 85–106.
Murray, J.W. (2006) *Ecology and Applications of Benthic Foraminifera*. New York: Cambridge University Press, p. 426.
Pantaléon-Cano, J., Yll, E.I., Pérez-Obiol, R. & Roure, J.M. (2003) Palynological evidence for vegetational history in semi-arid areas of the western Mediterranean (Almería, Spain). *The Holocene*, 13, 109–119.
Perçin Paçal, F. (2011) The ecology of the Ostracoda (Crustacea) species obtained from the coasts of Iskenderun Bay (Eastern Mediterranean Sea). *Journal of Black Sea/Mediterranean Sea Environment*, 17, 127–144.
Pint, A., Seeliger, M., Frenzel, P., Feuser, S., Erkul, E., Berndt, C. et al. (2015) The environs of Elaia's ancient open harbour – a reconstruction based on microfaunal evidence. *Journal of Archaeological Science*, 54, 340–355. Available at: https://doi.org/10.1016/j.jas.2014.06.011
Pirazzoli, P.A., Laborel, J., Saliège, J.F., Erol, O., Kayan, İ. & Person, A. (1991) Holocene raised shorelines on the Hatay coasts (Turkey): palaeoecological and tectonic implications. *Marine Geology*, 96, 295–311.
Pirazzoli, P.A., Laborel, J. & Stiros, S.C. (1996) Earthquake clustering in the Eastern Mediterranean during historical times. *Journal of Geophysical Research: Solid Earth*, 101, 6083–6097.
Polosa, A., Kızılarslanoğlu, H.A. & Oral, M. (Eds.) (2019) *Sebaste. Studies in Honour of Eugenia Equini Schneider*, Istanbul, Ege Yayinlari, p. 443.
Py, V., Véron, A., Edouard, J.L., Beaulieu, J.L., Ancel, B., Segard, M. et al. (2014) Interdisciplinary Characterisation and Environmental Imprints of Mining and Forestry in the Upper Durance Valley (France) During the Holocene. *Quaternary International*, 353, 74–97. Available at: https://doi.org/10.1016/j.quaint.2014.05.002
Rossi, V., Amorosi, A., Marchesini, M., Marvelli, S., Cocchianella, A., Lorenzini, L. et al. (2021) Late quaternary landscape dynamics at the La Spezia Gulf (NW Italy): a multi-proxy approach reveals environmental variability within a Rocky Embayment. *Water*, 13, 427. Available at: https://doi.org/10.3390/w13040427
Ruiz, F., Abad, M., Olías, M., Galán, E., González, I., Aguilá, E. et al. (2006) The present environmental scenario of the Nador Lagoon (Morocco). *Environmental Research*, 102, 215–229.
Ruiz, F., González-Regalado, M.L., Baceta, J.I., Menegazzo-Vitturi, L., Pistolato, M., Rampazzo, G. et al. (2000) Los ostrácodos actuales de la laguna de Venecia (NE de Italia). *Geobios*, 33, 447–454.
Russo Ermolli, E., Romano, P., Ruello, M.R. & Barone Lumaga, M.R. (2014) The natural and cultural landscape of Naples (southern Italy) during the Graeco-Roman and late antique periods. *Journal of Archaeological Science*, 42, 399–411, Available at: https://doi.org/10.1016/j.jas.2013.11.018
Şafak, Ü., Kelling, G., Gökçen, N.S. & Gürbüz, K. (2005) The mid-Cenozoic succession and evolution of the Mut Basin, southern Turkey, and its regional significance. *Sedimentary Geology*, 173(1-4), 121–150.
Salomon, F., Keay, S., Carayon, N. & Goiran, J.P. (2016) The development and characteristics of ancient harbours—applying the PADM chart to the case studies of Ostia and Portus. *PLoS One*, 11(9), e0162587. Available at: https://doi.org/10.1371/journal.pone.0162587
Salvi, G., Acquavita, A., Celio, M., Ciriaco, S., Cirilli, S., Fernetti, M. et al. (2020) Ostracod Fauna: eyewitness to fifty years of anthropic Impact in the Gulf of Trieste. A potential key to the future evolution of urban ecosystems. *Sustainability*, 12, 6954. Available at: https://doi.org/10.3390/su12176954
Salvi, G., Buosi, C., Arbulla, D., Cherchi, A., De Giudici, G., Ibba, A. et al. (2015) Ostracoda and foraminifera response to a contaminated environment: the case of the Ex-Military Arsenal of the La Maddalena Harbour (Sardinia, Italy). *Micropaleontology*, 61, 115–133.
Sayre, E.V., Joel, E.C., Blackman, M.J., Yener, K.A. & Özbal, H. (2001) Stable lead isotope studies of Black Sea anatolian ore sources and related bronze age and phrygian artefacts from nearby archaeological sites. Appendix: new central Taurus ore data. *Archaeometry*, 43(1), 77–115.
Schweingruber, F.H. (1990) *Anatomy of European Woods: An Atlas for the Identification of European Trees, Shrubs and Dwarf Shrubs*. Switzerland: Paul Haupt.
Seeliger, M., Brill, D., Feuser, S., Bartz, M., Erkul, E., Kelterbaum, D. et al. (2014) The purpose and age of underwater walls in the Bay of Elaia of Western Turkey: a multidisciplinary approach. *Geoarchaeology*, 29, 138–155.
Sgarrella, F. & Moncharmont Zei, M. (1993) Benthic foraminifera of the Gulf of Naples (Italy): systematics and autoecology. *Bollettino della Società Paleontologica Italiana*, 32, 145–264.
Shumilovskikh, L.S., Seeliger, M., Feuser, S., Novenko, E., Schlütz, F., Pint, A. et al. (2016) The harbour of Elaia: a palynological archive for human environmental interactions during the last 7500 years. *Quaternary Science Reviews*, 149, 167–187.
Silva-Sánchez, N. & Armada, X.L. (2023) Environmental impact of roman mining and metallurgy and its correlation with the archaeological evidence: a European perspective. *Environmental Archaeology*, 1–25. Available at: https://doi.org/10.1080/14614103.2023.2181295
Stock, F., Knipping, M., Pint, A., Ladstätter, S., Delile, H., Heiss, A.G. et al. (2016) Human impact on Holocene sediment dynamics in the Eastern Mediterranean – the example of the Roman harbour of Ephesus. *Earth Surface Processes and Landforms*, 41, 980–996.
Stock, F., Pint, A., Horejs, B., Ladstätter, S. & Brückner, H. (2013) In search of the harbours: new evidence of Late Roman and Byzantine harbours of Ephesus. *Quaternary International*, 312, 57–69.
Stock, F., Seyer, M., Symanczyk, A., Uncu, L., Brückner, H. (2020) On the geoarchaeology of Limyra (SW Anatolia)—new insights into the famous Lycian city and its environs. *Geoarchaeology*, 35, 487–502. Available at: https://doi.org/10.1002/gea.21781
Susini, D., Vignola, C., Goffredo, R., Totten, D.M., Masi, A., Smedile, A. et al. (2023) Holocene palaeoenvironmental and human settlement evolution in the southern margin of the Salpi lagoon, Tavoliere coastal plain (Apulia, Southern Italy). *Quaternary International*, 655, 37–54. Available at: https://doi.org/10.1016/j.quaint.2022.10.012
Tempesta, C., Pipere, M.-F. & Cassiani, V. (2020) Under the Auspices of Aphrodite Euploia: Port Infrastructure and Urban Transformation at Elaiussa Sebaste from the Hellenistic to Byzantine Age. In: Equini Schneider, E. (Ed.), *Men, Goods and Ideas Travelling over the Sea: Cilicia at the Crossroad of Eastern Mediterranean Trade Network*, Proceedings of the 19th International Congress of Classical Archaeology Cologne/Bonn, 22–26 May 2018 *Archaeology and Economy in the Ancient World*, 35, Heidelberg, pp. 39–52.
Toro, B. & Di Filippo, M. (1999) Caratteri fisiografici del territorio. In: Equini Schneider, E. (Ed.) *Elaiussa Sebaste I. Campagne di scavo 1995-1997*. Roma, Italy: L'Erma di Bretschneider. pp. 13–25.
Tsourou, T. (2012) Composition and distribution of recent Marine Ostracod Assemblages in the bottom sediments of Central Aegean Sea (SE Andros Island, Greece). *International Review of Hydrobiology*, 97, 276–300. Available at: https://doi.org/10.1002/iroh.201211492
Véron, A., Goiran, J.P., Morhange, C., Marriner, N. & Empereur, J.Y. (2006) Pollutant lead reveals the pre-Hellenistic occupation and ancient growth of Alexandria, Egypt. *Geophysical Research Letters*, 33(6), 1–4.
Véron, A.J., Flaux, C., Marriner, N., Poirier, A., Rigaud, S., Morhange, C. et al. (2013) A 6000-year geochemical record of human activities from Alexandria (Egypt). *Quaternary Science Reviews*, 81, 138–147. Available at: https://doi.org/10.1016/j.quascirev.2013.09.029
Vignola, C., Bonetto, J., Furlan, G., Mazza, M., Nicosia, C., Russo Ermolli, E. et al. (2022) At the origins of Pompeii: the plant landscape of the Sarno River floodplain from the first millennium BC to the AD 79 eruption. *Vegetation History and Archaeobotany*, 31(2), 171–186.
Vittori, C., Mazzini, I., Salomon, F., Goiran, J.P., Pannuzi, S., Rosa, C. et al. (2015) Palaeoenvironmental evolution of the ancient lagoon of Ostia Antica (Tiber delta, Italy). *Journal of Archaeological Science*, 54, 374–384. Available at: https://doi.org/10.1016/j.jas.2014.06.017
Wentworth, C.K. (1922) A scale of grade and class terms for clastic sediments. *The Journal of Geology*, 30, 377–392.
World register of marine species (WoRMS), Editorial Board. (2024) Available at: https://www.marinespecies.org. Accessed 2024-03-20.
Yassini, I. (1979) The littoral system ostracodes from the Bay of Bou-Ismail, Algiers, Algeria. *Revista española de micropaleontología*, XI(3), 353–416.
Zohary, M. (1962) *Plant Life of Palestine: Israel and Jordan*. New York: Ronald Press, 262 pp.